Stem Cell Reports
Article

OPEN ACCESS

Cell Surface N-Glycans Influence Electrophysiological Properties and Fate Potential of Neural Stem Cells

Andrew R. Yale,[1,2,3,8] Jamison L. Nourse,[2,3,8] Kayla R. Lee,[2,3] Syed N. Ahmed,[2,3] Janahan Arulmoli,[3,4] Alan Y.L. Jiang,[3,4] Lisa P. McDonnell,[2,3] Giovanni A. Botten,[5] Abraham P. Lee,[4] Edwin S. Monuki,[3,6] Michael Demetriou,[2,7] and Lisa A. Flanagan[1,2,3,4,*]

[1]Department of Anatomy & Neurobiology, University of California, Irvine, Irvine, CA 92697, USA
[2]Department of Neurology, University of California, Irvine, Irvine, CA 92697, USA
[3]Sue & Bill Gross Stem Cell Research Center, University of California, Irvine, Irvine, CA 92697, USA
[4]Department of Biomedical Engineering, University of California, Irvine, Irvine, CA 92697, USA
[5]Department of Microbiology, Immunology & Molecular Genetics, University of California, Los Angeles, Los Angeles, CA 90095, USA
[6]Department of Pathology and Laboratory Medicine, University of California, Irvine, Irvine, CA 92697, USA
[7]Department of Microbiology and Molecular Genetics, University of California, Irvine, Irvine, CA 92697, USA
[8]Co-first author
*Correspondence: lisa.flanagan@uci.edu
https://doi.org/10.1016/j.stemcr.2018.08.011

SUMMARY

Understanding the cellular properties controlling neural stem and progenitor cell (NSPC) fate choice will improve their therapeutic potential. The electrophysiological measure whole-cell membrane capacitance reflects fate bias in the neural lineage but the cellular properties underlying membrane capacitance are poorly understood. We tested the hypothesis that cell surface carbohydrates contribute to NSPC membrane capacitance and fate. We found NSPCs differing in fate potential express distinct patterns of glycosylation enzymes. Screening several glycosylation pathways revealed that the one forming highly branched N-glycans differs between neurogenic and astrogenic populations of cells *in vitro* and *in vivo*. Enhancing highly branched N-glycans on NSPCs significantly increases membrane capacitance and leads to the generation of more astrocytes at the expense of neurons with no effect on cell size, viability, or proliferation. These data identify the N-glycan branching pathway as a significant regulator of membrane capacitance and fate choice in the neural lineage.

INTRODUCTION

Neural stem cells (NSCs) develop into neurons, astrocytes, and oligodendrocytes and understanding how choices are made among these different fates will improve the use of these cells in transplantation therapies (Cao et al., 2002). NSCs expanded *in vitro* for therapeutic purposes generate a heterogeneous population of neural stem and progenitor cells (NSPCs) with varying ratios of progenitors linked to distinct cell fates. The cell biological characteristics that distinguish cells biased toward forming neurons from those that will generate astrocytes are ill-defined and current cell surface markers limited. Understanding the intrinsic properties of neuron- and astrocyte-biased cells and the mechanisms that govern their fate will improve the ability to predict or control the differentiation potential of transplanted cells, enhancing the reproducibility and effectiveness of NSPC therapeutics.

A cell biological characteristic that predicts fate in many stem cell lineages is whole-cell membrane capacitance, an electrophysiological property of the plasma membrane. Whole-cell membrane capacitance can be used to identify and enrich cells at distinct stages of differentiation and is measured for living cells, non-invasively, without labels by dielectrophoresis (DEP) or impedance sensing. Analysis or sorting of NSPCs by DEP is not toxic since the short-term DEP exposure needed for these applications does not alter cell survival, proliferation, or differentiation (Lu et al., 2012). Membrane capacitance discriminates between undifferentiated cells and their differentiated progeny. NSPCs are distinguished from differentiated neurons and astrocytes and prospectively sorted from neurons by membrane capacitance using DEP (Flanagan et al., 2008; Prieto et al., 2012). Membrane capacitance defines and enables the enrichment of undifferentiated and differentiated cells in the hematopoietic stem cell, mesenchymal stem cell (MSC)/adipose-derived stem cell, and embryonic stem cell lineages, indicating the relevance of biophysical properties to fate across multiple stem cell types (for a recent review see Lee et al., 2018).

For NSCs and MSCs, inherent electrophysiological properties of undifferentiated cells predict their differentiated fate. The neurogenic and astrogenic fate potential of NSPC populations (both human and mouse) are reflected in distinct membrane capacitance values, and membrane capacitance dynamically reflects the declining neurogenic potential of human NSPCs (Labeed et al., 2011). Importantly, the sufficiency of membrane capacitance as a marker of fate in the neural lineage is shown by the enrichment of neurogenic or astrogenic cells from a mixed population of undifferentiated mouse NSPCs by DEP (Nourse

et al., 2014; Simon et al., 2014). Similarly, the osteogenic fate potential of undifferentiated MSCs is detected by DEP (Hirota and Hakoda, 2011). Since the biophysical property whole-cell membrane capacitance is linked to fate, determining the components contributing to this measure may reveal novel insights into processes governing cell differentiation.

The cellular and molecular structures influencing membrane capacitance are not well understood. The DEP frequencies used for stem cell analysis are not in the range used to detect resting membrane potential (Gheorghiu, 1993; Flanagan et al., 2008). Expression of a G protein-coupled receptor in yeast did not alter capacitance (Stoneman et al., 2007), although expression of channelrhodopsin-2 in HEK293 cells did (Zimmermann et al., 2008), suggesting the possibility that certain membrane proteins can affect membrane capacitance. Based on biophysical theory, membrane capacitance should be impacted by plasma membrane surface area and thickness. While NSPCs that have distinct membrane capacitance values do not differ in size as measured by phase contrast microscopy (Labeed et al., 2011; Nourse et al., 2014), they may differ in membrane microdomains not visible at that level of resolution. Cell membrane microdomains such as ruffles or microvilli are expected to alter membrane capacitance by increasing cell surface area (Wang et al., 1994). Membrane thickness affected by the lipid composition of the plasma membrane has been proposed to influence whole-cell membrane capacitance, although there are constraints on the absolute thickness of the lipid bilayer set by the size of phospholipid head groups and fatty acid tails (Muratore et al., 2012). Modification of vesicle phospholipid bilayers with polyethylene glycol altered membrane capacitance (Desai et al., 2009), suggesting that cell surface modifications could contribute to membrane capacitance of cells.

A cellular process that modifies the plasma membrane surface and impacts membrane microdomains is glycosylation, by which carbohydrates able to store charge are added to plasma membrane proteins and lipids. Domains of glycosylated cell surface molecules generate surface undulations to increase surface area (Zhao et al., 2002), create structures extending up to 200 nm from the cell surface to make "thickened" membrane structures (Paszek et al., 2014), and influence the protein makeup of the plasma membrane (Nabi et al., 2015). Glycosylation is critical for normal nervous system development (Haltiwanger and Lowe, 2004), and changes in glycosylation patterns during cortical brain development correlate with developmental periods of increased neuron or astrocyte production (Flaris et al., 1995; Ishii et al., 2007). Treatment of NSPCs with agents that modify cell surface carbohydrates alters their behavior in DEP (Nourse et al., 2014), leading to the hypothesis that glycosylation may impact membrane capacitance and the fate of NSPCs.

RESULTS

Neurogenic and Astrogenic NSPCs Exhibit Differences in Glycosylation Enzymes

In the developing cerebral cortex, neurons are formed early (starting in mice at approximately embryonic day 10 [E10]) and neurogenesis decreases as astrocyte generation commences (around E16). Neurons and astrocytes are generated from NSPCs in the developing dorsal telencephalon stem cell niche (the ventricular zone/subventricular zone). In contrast, most cortical oligodendrocytes are generated ventrally in the ganglionic eminence and migrate into the cortex at later developmental stages (He et al., 2001). To test whether glycosylation patterns vary with fate potential, we isolated NSPCs from embryonic dorsal forebrain at stages when either more neurons (E12) or astrocytes (E16) are formed (Qian et al., 2000). E12 neuron-biased and E16 astrocyte-biased cells differ in fate-specific membrane capacitance, making these cells reasonable tests for the contribution of glycosylation to this biophysical property (Labeed et al., 2011).

Glycosylation is controlled by enzymes in the endoplasmic reticulum (ER) and Golgi that sequentially add and remodel sugars (glycans) attached to proteins and lipids destined for expression on the cell surface or extracellular secretion. We compared RNA levels of glycosylation enzymes in E12 and E16 NSPCs and found multiple differentially expressed genes (Tables S1–S3). Since membrane capacitance reflects characteristics of the plasma membrane, we prioritized enzymes expected to generate cell surface glycans, so enzymes involved in ER quality control, targeting of enzymes to lysosomes, or lysosomal degradation of glycans were not considered further. We focused on N-glycosylation since virtually all cell surface proteins are N-glycosylated and N-glycosylation controls function of membrane receptors mediating responses to extracellular cues. Loss of N-glycosylation enzymes causes defects in neural development (Schachter, 2001). N-Glycosylation leads to formation of membrane microdomains affecting cell surface area, which is thought to impact capacitance. Most O-glycosylated proteins are secreted and many become components of the extracellular matrix (ECM), but some, such as the heparan sulfate proteoglycans glypican and syndecan, can be membrane bound. Contributions of O-glycosylation to membrane capacitance and the combined effects of N- and O-glycosylation will be the focus of future studies.

N-Glycosylation enzymes exhibiting a 1.2-fold or greater difference in expression between E12 and E16 NSPCs can

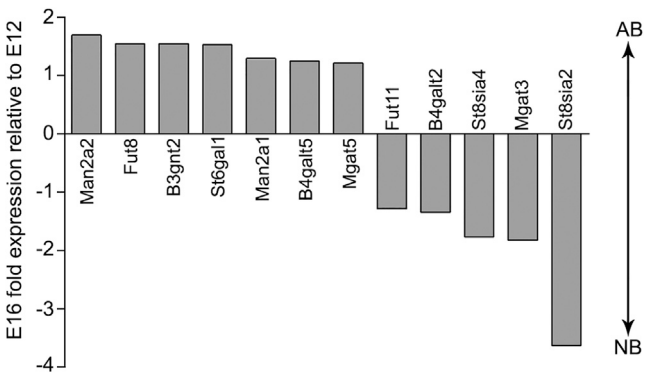

Figure 1. Differences in N-Glycosylation Enzyme Gene Expression between E12 and E16 Mouse NSPCs

Thirty-two N-glycosylation enzyme genes were screened and 12 transcripts differed by more than 1.2-fold; 7 were higher in E16 astrocyte-biased (AB) NSPCs while 5 were higher in E12 neuron-biased (NB) NSPCs.

be grouped by function (Figure 1). N-Acetylglucosaminyltransferases (MGAT3 and MGAT5), along with mannosidase II (MAN2A1 and MAN2A2), determine the degree of N-glycan branching. Sialyltransferases include ST6GAL1, which generates a terminal sialic acid, and ST8SIA2 and ST8SIA4 that work together to form polysialic acid. FUT8 and FUT11 are fucosyltransferases that add fucose residues to the core or terminal ends of N-glycans, respectively. B4GALT2 and B4GALT5 are galactosyltransferases that add galactose to N-glycans. B3GNT2 is an acetylglucosaminyltransferase that adds N-acetylglucosamine (GlcNAc) to N-glycans. The N-glycan branching, sialic acid, and fucose pathways were assessed further to test their association with fate in the neural lineage since multiple members of these pathways were identified in the screen and enzymes that perform different functions were associated with either E12 or E16 NSPCs.

Complex Branching but Not Sialylation or Fucosylation Correlates with NSPC Fate

N-Glycan branching is controlled by enzymes that cleave excess mannose residues and initiate new N-glycan branches by attaching GlcNAc (Figure 2A). High-mannose N-glycans contain no GlcNAc branches, while hybrid N-glycans contain both mannose and GlcNAc, and complex N-glycans have lost all the excess mannose residues. RNA sequencing analysis revealed high expression of N-glycan branching genes, including *Man1* isoforms, *Man2* isoforms, *Mgat1, Mgat2, Mgat3, Mgat4* isoforms, and *Mgat5* (Figure 2B). NSPCs also express galectins, which bind N-glycans and modulate the activities of several N-glycan-containing cell surface proteins. NSPCs express galectins 1, 4, 5, and 8, but little to no 2, 3, 7, 9, or 12 (Figure 2B).

Gene expression analysis by qRT-PCR of *Mgat1*, the initial N-acetylglucosaminyltransferase in the pathway, and *Man2a1, Man2a2*, and *Mgat5*, identified in the initial screen (Figure 1), revealed significantly higher levels of *Mgat1* in E16 compared with E12 NSPCs (Figure S1A). MALDI-TOF mass spectrometry analysis suggested more N-glycans with one or two GlcNAc branches on E12 NSPCs but more with three or four branches on E16 cells (Figure S1B). Lectin flow cytometry with fluorescein-conjugated leukocyte-phytohemagglutinin (L-PHA), a plant lectin highly specific for MGAT5-generated highly branched tetra-antennary N-glycans (Cummings and Kornfeld, 1982), detected higher but not significantly different L-PHA binding on E16 NSPCs compared with E12 cells (Figure S1C).

We sorted E12 NSPCs by DEP to generate both control and astrocyte-biased populations (Nourse et al., 2014; Simon et al., 2014) from the same developmental stage since variation between E12 and E16 NSPCs could be due to their different ages independent of fate (Figure 2C). We tested enrichment by analyzing undifferentiated cells for markers of astrocyte progenitors (Hartfuss et al., 2001; Sun et al., 2005; Chaboub et al., 2016) and differentiated cells for the formation of GFAP-positive astrocytes. As expected, the astrocyte progenitor markers *Asef* (*Arghgef4*), *Glast* (*Slc1a3*), and *Egfr* were more highly expressed in undifferentiated E16 NSPCs than in E12 cells (Figure S1D). Expression of astrocyte progenitor markers in undifferentiated cells (Figure 2D) and GFAP-positive astrocytes after differentiation (Figure 2E) indicate that DEP sorting enriched astrocyte-biased cells. While some NSPCs express GFAP, control and sorted undifferentiated E12 NSPCs do not express GFAP (Figure S1E) (Flanagan et al., 2008), confirming that this marker can be used to detect astrocyte differentiation from these cells. Analysis of both undifferentiated and differentiated cells indicate that sorting generated a more astrocyte-biased population of cells (Figure 2).

We used qRT-PCR to screen for differences in glycosylation enzyme expression between control and sorted astrocyte-biased NSPCs. Sorted cells express significantly higher levels of *Man2a1, Man2a2*, and *Mgat5* and a trend toward higher *Mgat1* compared with unsorted E12 NSPCs (Figure 2F). Notably, sorted cells appear deficient in *Mgat3*, which prevents formation of highly branched N-glycans (Brockhausen et al., 1988) and was higher in E12 NSPCs than E16 NSPCs in the initial screen (Figures 1 and 2F). Furthermore, highly branched N-glycans detected by L-PHA were significantly elevated in sorted cells (MFI, 19,423 ± 2,023) compared with unsorted control NSPCs (MFI, 18,101 ± 2,092) (paired Student's t test, $p = 0.0157$). Together with the analysis of E12 and E16 NSPCs, the sorted cell data indicate a correlation between highly

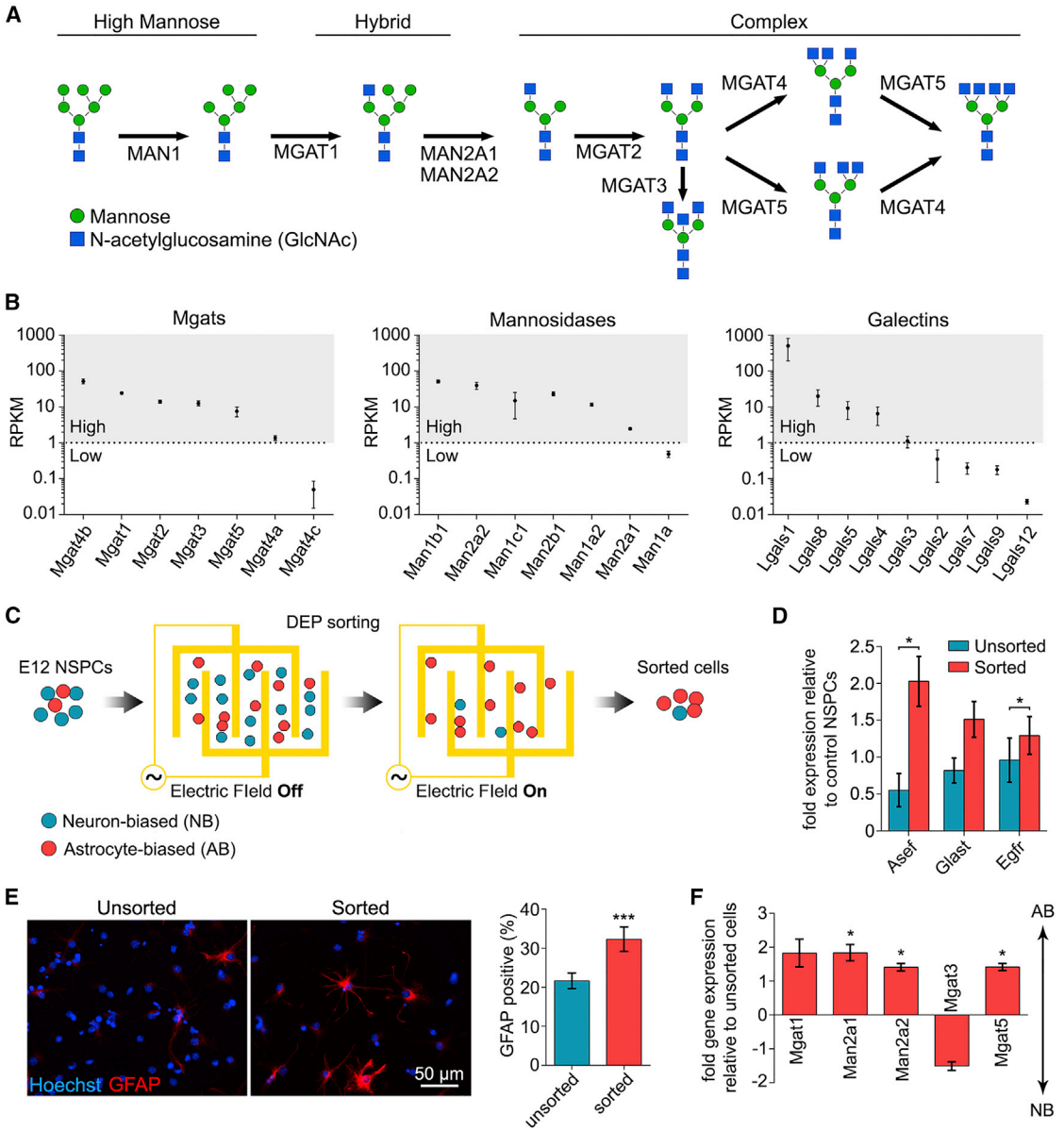

Figure 2. N-Glycan Branching Correlates with NSPC Fate

(A) Schematic representation of the N-glycans formed by glycosylation enzymes, culminating in the formation of highly branched, complex N-glycans.

(B) RNA sequencing analysis of E12 NSPCs. Average RPKM (reads per kilobase of transcript per million mapped reads) values are organized from high (>1 RPKM) to low (<1 RPKM) expression.

(C) In DEP sorting, E12 NSPCs are randomly distributed when the electric field is off. When the electric field is on, astrocyte-biased cells are attracted to electrode edges and neuron-biased cells are removed by flow, leaving an astrocyte-biased population of sorted cells.

(D) qRT-PCR analysis of astrocyte progenitor marker expression indicates that sorted cells have significantly increased *Asef* ($p = 0.0239$) and *Egfr* ($p = 0.0273$) expression (paired Student's t test).

(E) Sorted cells generate more GFAP-positive cells after differentiation ($p = 0.0002$, paired Student's t test).

(F) qRT-PCR analysis shows that sorted cells express higher levels of branching enzymes (*Man2a1*, $p = 0.0433$; *Man2a2*, $p = 0.0474$; *Mgat5*, $p = 0.0314$, paired Student's t test sorted versus unsorted), while *Mgat3* that prevents branching appears decreased.

All error bars represent SEM. N = 3 or more independent biological repeats (*$p < 0.05$, ***$p < 0.001$).

branched N-glycans and the fate of the cell population, suggesting that this pathway may affect membrane capacitance and fate in the neural lineage.

The three enzymes that add sialic acid to N-glycans identified in the original screen of E12 and E16 NSPCs were *St6gal1*, which had higher expression in E16 NSPCs, and *St8sia2* and *St8sia4*, which were more highly expressed in E12 NSPCs (Figure 1). Analysis by qRT-PCR indicated significantly higher levels of *St8sia2* and *St8sia4* in E12 NSPCs compared with E16 NSPCs, but no difference in *St6gal1* (Figure S2A). MALDI-TOF studies suggested higher levels of sialic acid containing N-glycans on E12 compared with E16 NSPCs (Figure S2B). Using the lectin *Sambucus nigra* agglutinin (SNA), we found no difference in terminal sialic acid residues generated by ST6GAL1 between E12 and E16 NSPCs (Figure S2C). ST8SIA2 and ST8SIA4 form long polysialic acid (PSA) chains, most notably on the neural cell adhesion molecule (NCAM) to generate PSA-NCAM. PSA-NCAM was detected at lower levels on E16 NSPCs compared with E12 cells, but the difference was not significant (Figure S2D). Neither *St8sia2* expression nor PSA-NCAM differed between the sorted astrocyte-biased population and unsorted NSPCs (Figures S2E and S2F). Thus, while there may be more sialic acid on E12 than E16 NSPCs, potentially via the activities of ST8SIA2 and ST8SIA4 but not ST6GAL1, the lack of a difference in *St8sia2* and PSA expression in the sorted cells suggests that this may not directly relate to fate. We previously found that isolation of PSA-NCAM-positive cells from E12 NSPCs did not enrich for neuron-generating cells (Nourse et al., 2014). Furthermore, treatment of blood cells with neuraminidase to remove sialic acid did not change cell responses in DEP frequency ranges that probe the plasma membrane, indicating that the loss of sialic acid did not affect membrane capacitance (Burt et al., 1990). While E12 NSPCs have higher levels of PSA-generating enzymes than E16 NSPCs, there is not a clear link between PSA and fate-specific membrane capacitance.

Fucosylation of N-glycans occurs through the activities of fucosyltransferases (FUTs). FUT8, which attaches a core fucose, showed the greatest difference in the original screen of E12 and E16 NSPCs and was higher in E16 cells (Figure 1). Analysis of E12 and E16 NSPCs by qRT-PCR showed slightly higher but not significantly different levels of *Fut8* in the E16 sample (Figure S3A), and core-fucosylated N-glycans were slightly elevated in E16 NSPC membranes compared with those from E12 as indicated by MALDI-TOF (Figure S3B). However, lectin flow cytometry with *Lens culinaris* agglutinin, which detects core-fucosylated N-glycans, indicated similar levels of core fucose on E16 NSPCs and E12 NSPCs (Figure S3C). In addition, *Fut8* expression did not differ between the unsorted control NSPCs and the sorted astrocyte-biased population (Figure S3D). Thus, the analysis of *Fut8* expression and activity in NSPCs did not provide evidence of a significant association between core fucosylation and fate in the neural lineage.

Highly Branched N-Glycans Increase in the Brain Stem Cell Niche as Fate Shifts from Neurogenesis to Astrogenesis

Development of the mammalian cerebral cortex proceeds in a stepwise pattern with neurons formed first (~E10 in mice) followed by astrocytes (~E16). The sequential generation of neurons and astrocytes provides a means to test the association of glycosylation with fate *in vivo*. Cortical NSPCs reside in the ventricular zone/subventricular zone (VZ/SVZ) of the embryonic cerebral cortex, and differentiated cells migrate away from this region toward the pial surface to form the cortical plate (CP). We analyzed sagittal brain sections from E10-E18 embryos and used the NSPC markers Sry-box (SOX) 1 and SOX2 to mark the VZ/SVZ and microtubule-associated protein 2 (MAP2) and doublecortin (DCX) as markers of differentiated neurons to define the CP (Figure S4). Oligodendrocytes are not primarily generated in the cortex; most form ventrally in the ganglionic eminence and migrate to inhabit the cortex (dorsal telencephalon) at later embryonic stages, ~E18 (He et al., 2001). Thus, very few oligodendrocyte progenitors would be present in the cortical stem cell niche.

We used L-PHA lectin staining to assess highly branched N-glycans in the VZ/SVZ stem cell niche and found significantly more L-PHA binding at E16 than at E12 (Figure 3). There was no difference in staining of the CP at E12 and E16, showing that the differences in the VZ/SVZ were not due to general increases in highly branched N-glycans in all regions of the cortex over time. The levels of highly branched N-glycans continue to increase in the VZ/SVZ NSPC niche at E18 as astrogenesis escalates (Figures 3C, 3D, and S5). Together with the results from cell culture studies, these data show that highly branched N-glycans are associated with astrogenic NSPC populations both *in vitro* and *in vivo*.

GlcNAc Treatment Enhances Expression of Highly Branched N-Glycans on E12 NSPCs and Significantly Increases Membrane Capacitance

We tested whether altering highly branched N-glycans on the surface of E12 NSPCs changes their membrane capacitance values by supplementing the cells with GlcNAc, which is readily taken up by cells and raises intracellular UDP-GlcNAc levels. The MGAT4 and MGAT5 branching enzymes are highly sensitive to availability of UDP-GlcNAc, and GlcNAc treatment increases N-glycan branching in a variety of cell types (Lau et al.,

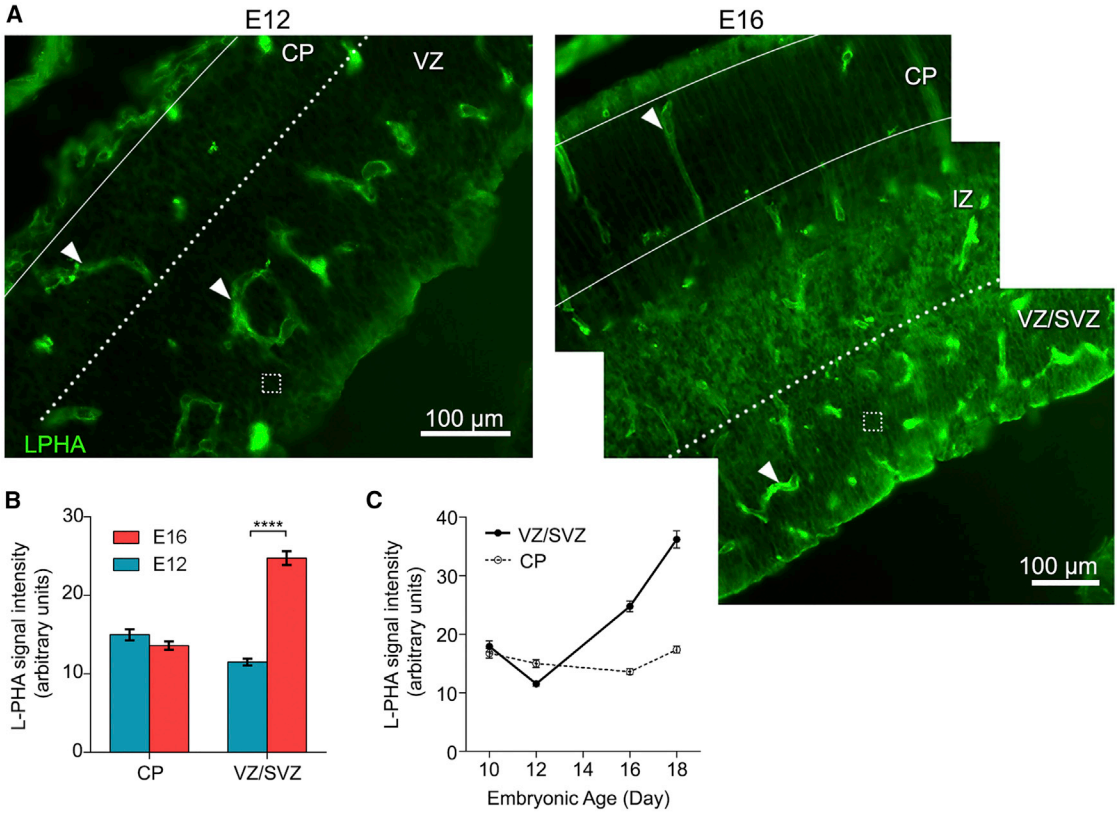

D

Cortical Plate

comparison	p-value	significance
E10 vs. E12	0.2628	ns
E10 vs. E16	0.0046	**
E10 vs. E18	0.9208	ns
E12 vs. E16	0.4619	ns
E12 vs. E18	0.0735	ns
E16 vs. E18	0.0005	***

Ventricular/Sub-ventricular Zone

comparison	p-value	significance
E10 vs. E12	0.0001	***
E10 vs. E16	<0.0001	****
E10 vs. E18	<0.0001	****
E12 vs. E16	<0.0001	****
E12 vs. E18	<0.0001	****
E16 vs. E18	<0.0001	****

Figure 3. N-Glycan Branching in the Stem Cell Niche Is High during Astrogenic Developmental Stages *In Vivo*

(A) L-PHA indicates highly branched N-glycans in sagittal sections of the cerebral cortex at E12 and E16. Arrowheads point to blood vessels, which were excluded from analysis. Dotted boxes indicate example regions used for quantitative analysis (10 boxes or more were analyzed per layer in each section). More intense staining is evident in the E16 NSPC niche (VZ/SVZ) than the E12 niche (VZ).

(B) Significantly greater staining in the E16 NSPC niche but no difference in the CP (VZ/SVZ E12 versus E16, $p < 0.0001$; CP E12 versus E16, $p = 0.1041$, unpaired Student's t test).

(C) L-PHA staining increases in the NSPC niche (VZ/SVZ) from E10 to E18 without a corresponding increase in the CP.

(D) Statistical analysis of the data in (C) indicates a significant increase in L-PHA intensity in the VZ/SVZ over time ($p < 0.0001$, one-way ANOVA, Tukey *post hoc* for multiple comparisons; ns, not significant).

Error bars SEM. N = 3 or more independent biological repeats (**$p < 0.01$, ***$p < 0.001$, ****$p < 0.0001$).

2007). GlcNAc treatment significantly increased highly branched N-glycans detected by L-PHA on the surface of E12 NSPCs (Figure 4). Increasing cell surface highly branched N-glycans also caused a significant increase in whole-cell membrane capacitance of E12 NSPCs, indicating a role for branched N-glycans in membrane capacitance (Figure 4C).

Highly Branched N-Glycans Restrict Neurogenesis without Affecting NSPC Size, Viability, or Proliferation

Highly branched N-glycans may serve as markers of fate or may actively participate in fate decisions since glycosylation controls the function of myriad cell surface receptors, many with identified roles in fate decisions (Zhao et al.,

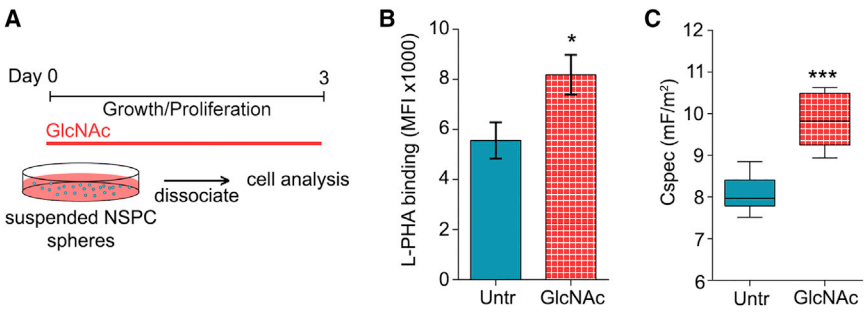

Figure 4. Enhancing N-Glycan Branching on the Cell Surface Increases NSPC Membrane Capacitance

(A) Experimental design: suspended undifferentiated E12 NSPCs were grown in proliferation medium supplemented with 80 mM GlcNAc for 3 days then dissociated for analysis.

(B) Flow cytometry with L-PHA indicates significantly more cell surface highly branched N-glycans on GlcNAc-treated cells compared with untreated (Untr) control cells ($p = 0.0219$, unpaired Student's t test). Error bars SEM.

(C) Whole-cell-specific membrane capacitance (Cspec) measured by DEP is significantly increased after GlcNAc treatment of E12 NSPCs ($p = 0.001$, unpaired Student's t test). Boxplots depict 25th and 75th quartiles and median, and the bars represent min and max values. mF, milliFarad.

N = 3 or more independent biological repeats (*$p < 0.05$, ***$p < 0.001$).

2008). We assessed neuronal differentiation of control and GlcNAc-treated E12 NSPCs to test whether highly branched N-glycans impact fate. GlcNAc treatment led to a dose-dependent decrease in neuron formation, with significantly lower neurogenesis after treatment with 40 or 80 mM GlcNAc (Figures 5A and 5B). There was no difference in cell size of control and 80 mM GlcNAc-treated NSPCs (Figure 5C), consistent with the fact that neither NSPCs that differ in fate (E12 and E16) nor astrocyte- and neuron-biased populations enriched from E12 NSPCs differ in size (Labeed et al., 2011; Nourse et al., 2014). GlcNAc supplementation might induce cell death, leading to the loss of cells biased to a particular fate. Yet there was no difference in cell viability or percentage of apoptotic cells between control and GlcNAc-treated NSPCs, suggesting that cell death does not play a role in the effect of highly branched N-glycans on fate (Figure 5D). Highly branched N-glycans could alter cell proliferation, impacting the percentage of neuron-biased cells in the population. However, two measures of cell proliferation (EdU incorporation and phosphorylated histone H3 expression) showed no differences between control and GlcNAc-treated NSPCs (Figure 5E). In sum, GlcNAc treatment to induce highly branched N-glycans on E12 NSPCs decreases neurogenesis but not by altering cell size, viability, or proliferation.

Enhancing Highly Branched N-Glycans on Undifferentiated NSPCs Leads to the Formation of More Astrocytes at the Expense of Neurons

GlcNAc treatment effects could be due to branched N-glycans on undifferentiated NSPCs, on newly differentiated cells, or a combination of both since GlcNAc treatment spanned proliferation and differentiation stages (Figure 5). Experiments were therefore designed to separate these effects by treating cells (1) when in the undifferentiated state (in proliferation medium), (2) as they differentiate (in differentiation medium), or (3) during both stages (throughout) (Figure 6A).

GlcNAc treatment throughout both proliferation and differentiation stages led to a significant decrease in neuron formation (Figures 6B and 6D, "throughout") as seen in our initial experiments of neuron differentiation (Figure 5). Treatment during only the proliferation stage induced a similar decrease in neuron formation, but treatment during the differentiation stage had no effect on the percentage of neurons (Figures 6B and 6D, "proliferation," "differentiation"). These data indicate that increasing cell surface highly branched N-glycans decreases the neurogenic potential of undifferentiated E12 NSPCs rather than affecting differentiated neurons.

Analysis of astrocyte generation from E12 NSPCs treated with GlcNAc revealed effects of highly branched N-glycans on both undifferentiated and differentiated cells. Astrocyte quantitation was standardized by analyzing regions that did not contain dense clusters of cells and cell debris (Figure S6) since astrocytes can become reactive in response to dying cells and upregulate GFAP expression, complicating analysis. GlcNAc treatment of undifferentiated NSPCs led to a significant increase in the percentage of astrocytes formed after differentiation (Figures 6C and 6E, proliferation). Interestingly, treatment during the differentiation stage also significantly increased astrocyte percentages, suggesting effects of highly branched N-glycans on the differentiated cells (Figures 6C and 6E, differentiation). The percentage of astrocytes formed when GlcNAc treatment occurred throughout both proliferation and differentiation stages was significantly higher than that of cells treated just during proliferation, suggesting an additive effect on both undifferentiated and differentiated cells (Figures 6C and 6E, throughout). Thus, highly branched

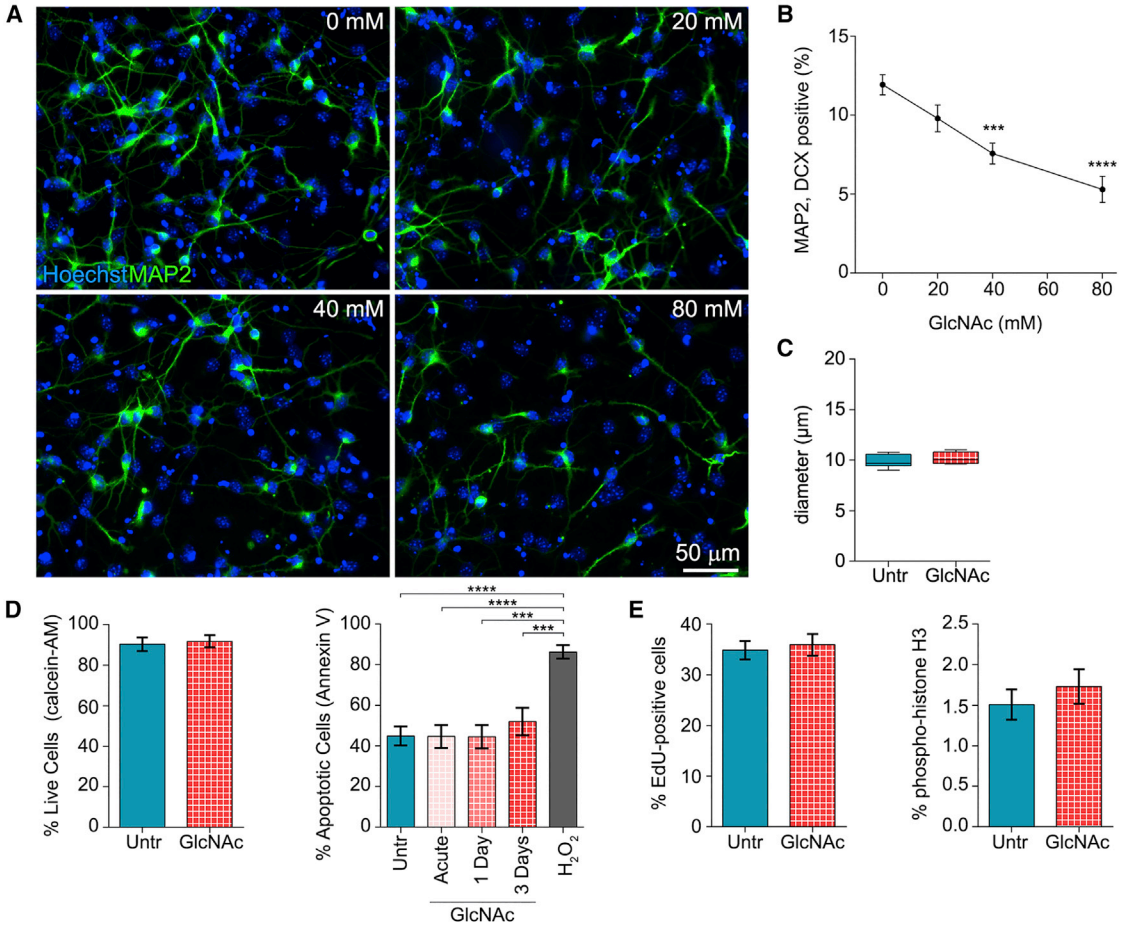

Figure 5. NSPCs with Enhanced Cell Surface N-Glycan Branching Form Fewer Neurons upon Differentiation but Do Not Differ in Size, Viability, or Proliferation

(A) Neuron formation (MAP2) from E12 NSPCs treated with 0–80 mM GlcNAc for 3 days as undifferentiated cells and 3 days during differentiation. All nuclei labeled with Hoechst.

(B) The percentage of MAP2/doublecortin (DCX) double-positive neurons formed from E12 NSPCs decreases with increasing GlcNAc concentration (one-way ANOVA, $p < 0.0001$). *Post hoc* analysis by Dunnett's test: untreated E12 NSPCs versus 40 mM ($p = 0.0002$) and 80 mM ($p < 0.0001$) GlcNAc-treated cells.

(C) Treatment with 80 mM GlcNAc did not alter cell diameters of E12 NSPCs ($p = 0.3985$, unpaired Student's t test).

(D) Cell viability live/dead assay denotes no effect of 80 mM GlcNAc treatment on the percentage of live E12 NSPCs ($p = 0.7569$, unpaired Student's t test). Annexin V flow cytometry indicated no difference in apoptosis acutely (~3–6 hr post treatment), 1 day, or 3 days after GlcNAc supplementation. Positive control cells were treated with 200 µM H_2O_2 for 3 hr to induce apoptosis.

(E) NSPC proliferation measured by EdU incorporation (cells in S-phase) and phospho-histone H3 staining (cells in M-phase) was not affected by 80 mM GlcNAc treatment (EdU $p = 0.7023$, phospho-histone H3 $p = 0.4354$, unpaired Student's t tests).

Error bars SEM. N = 3 or more independent biological repeats (***$p < 0.001$, ****$p < 0.0001$).

N-glycans impact the formation of astrocytes from NSPCs and also affect differentiated astrocytes.

At E12, cortical NSPCs primarily generate neurons and astrocytes, and the number of cells in the cortex capable of making oligodendrocytes is low, in part since very few oligodendrocyte-producing cells have migrated from the ganglionic eminence into the cortex at this stage (He et al., 2001). However, since E12 cortical NSPCs can generate low numbers of oligodendrocytes in culture (Qian et al., 2000), we assessed the effects of GlcNAc on oligodendrocyte generation. Oligodendrocyte percentages were significantly decreased when cells were treated with 80 mM GlcNAc during proliferation or throughout both proliferation and differentiation stages, but not when treated during differentiation only (Figure S7). Since E12 NSPCs generate few oligodendrocytes, the biological

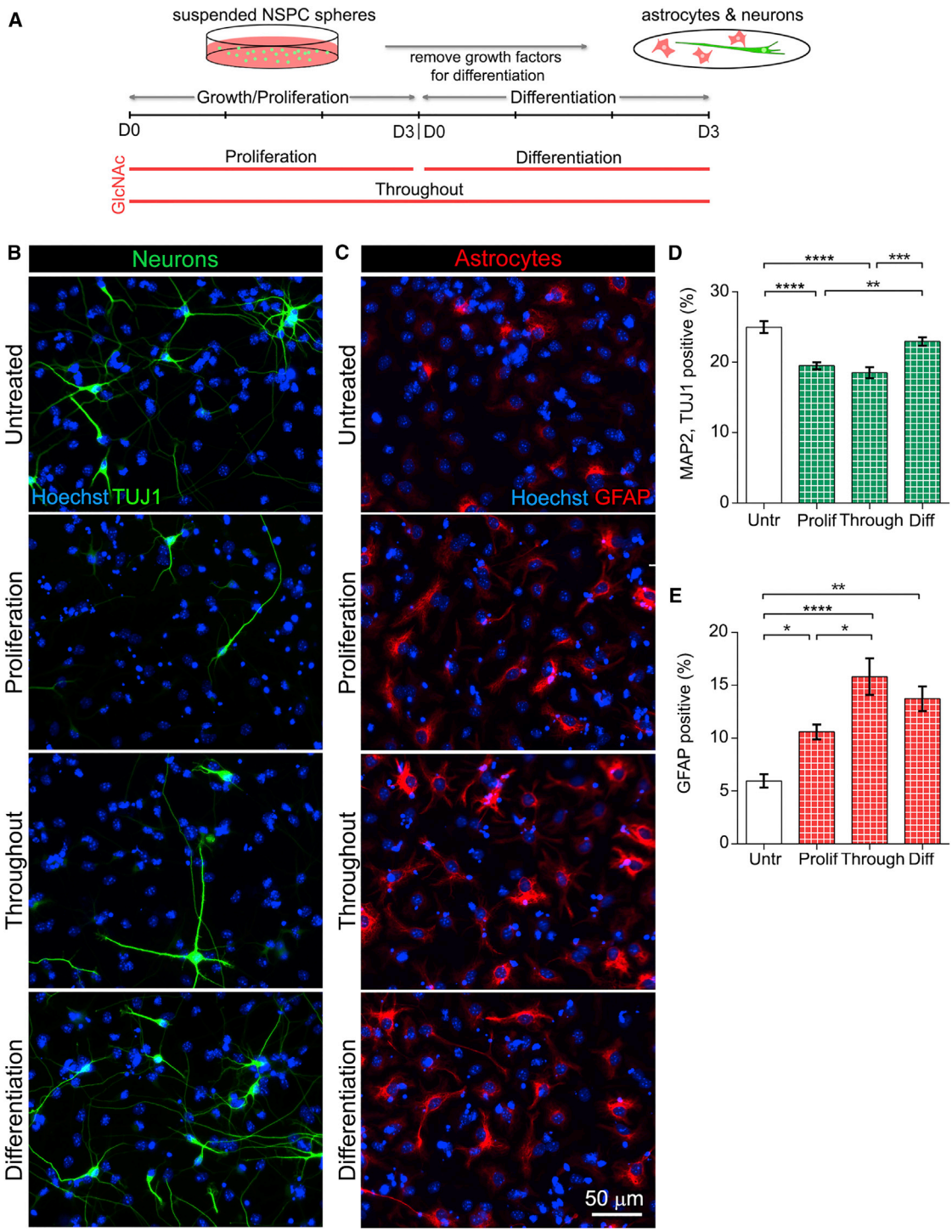

Figure 6. Increasing N-Glycan Branching on Undifferentiated NSPCs Decreases Neurogenesis and Increases Astrogenesis upon Differentiation

(A) Experimental design: E12 NSPCs were treated with 80 mM GlcNAc in proliferation medium (undifferentiated cells, Proliferation, 3 days treatment), in differentiation medium (as cells differentiate, Differentiation, 3 days treatment), or in both proliferation and differentiation (Throughout, 6 days treatment). Cells were in suspension during the proliferation stage then plated as adherent cells on laminin for differentiation.

(legend continued on next page)

significance of this finding is unclear, and further analysis should utilize cells isolated from the ganglionic eminence or other means to assess cells capable of generating higher numbers of oligodendrocytes.

GlcNAc is utilized in both N- and O-glycosylation, so we tested whether GlcNAc effects were specifically due to incorporation in N-glycan branching by pretreating cells with kifunensine (Kif). Kif is a highly specific inhibitor of mannosidase I and blocks the first steps of N-glycan branching (Figure 2A) (Males et al., 2017). E12 NSPCs were pre-treated with Kif and maintained in Kif during GlcNAc treatment to prevent GlcNAc incorporation into N-glycan branches (Figure 7A). As indicated by L-PHA flow cytometry, Kif effectively blocked branching since no increase in branched N-glycans occurred with GlcNAc in the presence of Kif (Figure 7B). No significant difference in neuron formation was observed between Kif-treated NSPCs and cells treated with both Kif and GlcNAc, indicating that Kif blocked the effect of GlcNAc on NSPC neurogenesis (Figure 7C). Similarly, Kif prevented the effect of GlcNAc on astrogenesis since the Kif-treated NSPCs did not differ from those treated with both Kif and GlcNAc (Figure 7D). The ability of Kif to block the effects of GlcNAc indicates that GlcNAc influences the fate potential of NSPCs through the formation of branched N-glycans.

DISCUSSION

We identify the N-glycosylation pathway leading to the formation of highly branched N-glycans as a regulator of fate choice in the neural lineage and provide links between the expression of N-glycans on the cell surface and membrane capacitance, a novel label-free biomarker of cell fate. Neurogenic and astrogenic NSPCs differ in expression of enzymes that lead to the formation of highly branched N-glycans, and these N-glycans increase in the stem cell niche *in vivo* as fate potential shifts from neurogenesis to astrogenesis. NSPCs induced to express more highly branched N-glycans had significantly increased fate-specific membrane capacitance values, providing a direct link between cell surface glycosylation and this biophysical property. Increasing the levels of NSPC highly branched N-glycans specifically affected fate choice since GlcNAc treatment led to the formation of greater percentages of astrocytes at the expense of neurons without affecting cell size, proliferation, or death. These data indicate that the N-glycan branching pathway is an important regulator of fate choice in the neural lineage.

Cell surface N-glycosylation significantly impacts membrane capacitance, a label-free measure of cell fate. Glycosylation likely affects capacitance values of many cell types since reductions in the complexity of the bacteria *C. difficile* S-layer, which is made up of glycoproteins and glycans on the bacterial envelope, induces shifts in membrane capacitance (Su et al., 2014). Glycosylation may contribute to membrane capacitance in other stem cell lineages; differentiation of MSCs to either adipogenic or osteogenic fates is associated with differences in both membrane capacitance (Bagnaninchi and Drummond, 2011) and glycosylation (Heiskanen et al., 2009; Hamouda et al., 2013). The interaction of membrane capacitance, cell fate, and cell surface glycosylation may have relevance for many cell types, including those in other stem cell lineages.

Cell surface glycosylation affects membrane structure and surface area, which are expected to impact whole-cell membrane capacitance (Wang et al., 1994). The size of neuron- and astrocyte-biased NSPCs enriched by DEP did not differ (Nourse et al., 2014) and there was no difference in the size of untreated and GlcNAc-treated NSPCs in phase contrast microscopy although they differ in both membrane capacitance and fate (e.g., Figures 4, 5, and 6). Cell surface glycosylation affects the formation of membrane microdomains such as microvilli and lipid rafts associated with membrane invaginations, and thus could lead to changes in surface area not visible by phase contrast (Zhao et al., 2002; Garner and Baum, 2008). The cell surface glycocalyx (glycoproteins, glycolipids, and galectins) can create thickened regions of membrane that may affect capacitance (Paszek et al., 2014). The shift in membrane capacitance of E12 NSPCs due to GlcNAc treatment (untreated: 8.2 ± 0.2 mF/m^2; GlcNAc

(B) Fewer neurons formed from GlcNAc-treated NSPCs during proliferation or throughout both stages compared with cells treated during differentiation or untreated controls. No obvious differences in neuronal morphology were noted in the different conditions.
(C) More astrocytes were generated from GlcNAc-treated NSPCs than untreated controls (all treatment paradigms).
(D) Significantly reduced MAP2/TUJ1 double-positive neurons from cells treated with GlcNAc during proliferation (Prolif) or throughout both stages (Through) compared with cells treated during differentiation (Diff) or untreated (Untr) control cells (Untr versus Prolif $p < 0.0001$, Untr versus Through $p < 0.0001$, Prolif versus Diff $p = 0.0042$, Through versus Diff $p = 0.0002$, one-way ANOVA, Tukey *post hoc* for multiple comparisons). These data indicate an effect of GlcNAc on undifferentiated NSPCs but not on differentiated neurons.
(E) The percentage of GFAP-positive astrocytes was significantly increased in all GlcNAc-treated samples, showing effects of N-glycan branching on both undifferentiated NSPCs and differentiated cells (Untr versus Prolif $p = 0.047$, Untr versus Through $p < 0.0001$, Untr versus Diff $p = 0.0018$, Prolif versus Through $p = 0.0236$, one-way ANOVA, Tukey *post hoc* for multiple comparisons).
Error bars SEM. N = 3 or more independent biological repeats (*$p < 0.05$, **$p < 0.01$, ***$p < 0.001$, ****$p < 0.0001$).

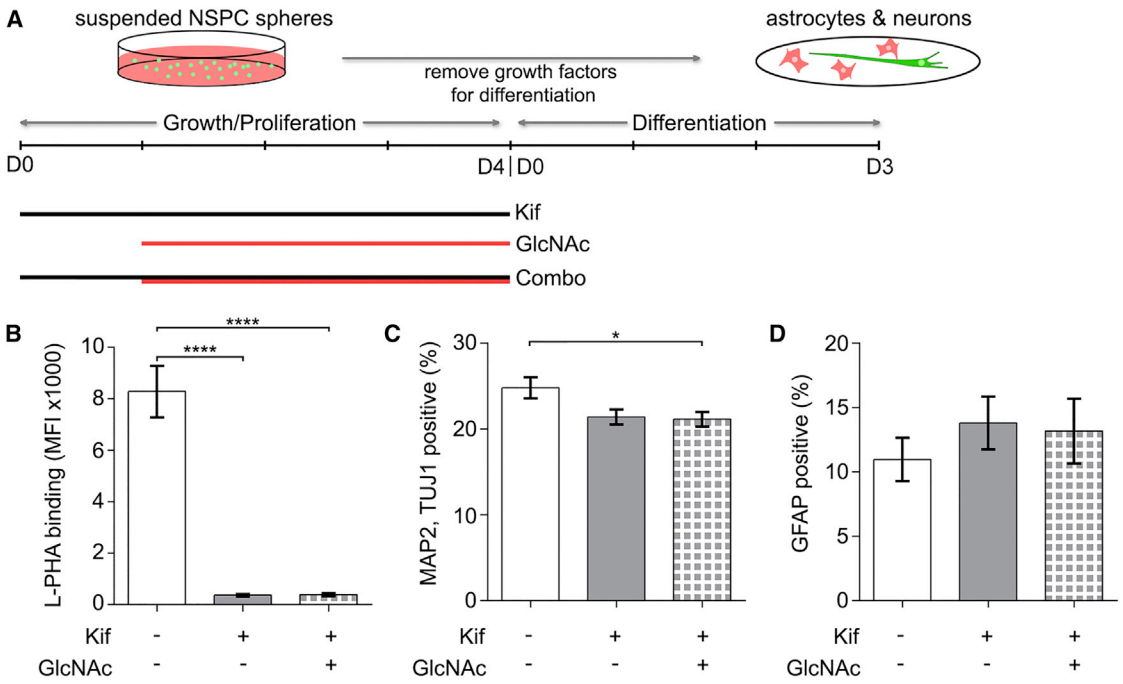

Figure 7. Preventing GlcNAc from Incorporating into the N-Glycan Branching Pathway Blocks GlcNAc Effects on Fate Potential

(A) Experimental design: Undifferentiated E12 NSPCs were treated with either 0.5 μM Kif for 4 days, 80 mM GlcNAc for 3 days, or pre-treated with Kif 1 day prior to an additional 3 days of Kif + GlcNAc supplementation (Combo). Cells were differentiated for 3 days after treatment.

(B) L-PHA flow cytometry analysis of cells after the 4 days of treatment indicates significantly lower highly branched N-glycans on Kif- and Combo-treated cells compared with untreated controls (untreated versus Kif or Combo $p < 0.0001$, one-way ANOVA, Tukey *post hoc* for multiple comparisons).

(C) No difference in neuronal differentiation between Kif- and Combo-treated cells, indicating no effect of GlcNAc in the presence of Kif. Combo-treated cells show a slight decrease in neuron formation compared with untreated controls (untreated versus Combo $p = 0.0311$, one-way ANOVA, Tukey *post hoc* for multiple comparisons).

(D) When blocked by Kif, GlcNAc has no effect on astrocyte formation since no difference was observed between Kif- and Combo-treated samples.

Error bars SEM. N = 3 or more independent biological repeats (*$p < 0.05$, ****$p < 0.0001$).

treated: 9.8 ± 0.3 mF/m^2) (Figure 4) is similar to the difference in membrane capacitance values of E12 and E16 NSPCs that differ in fate (E12: 8.2 ± 0.5 mF/m^2; E16: 10.7 ± 0.6 mF/m^2) (Labeed et al., 2011). Thus, cell surface highly branched N-glycans could be sufficient to explain the fate-specific differences in capacitance of NSPCs.

Increasing highly branched N-glycans on NSPCs alters fate potential, leading to the generation of more astrocytes and fewer neurons while not inducing changes in cell proliferation or viability. A direct role for branched N-glycans in NSPC differentiation has not been previously described, although glycosylation patterns shift in the cortex during developmental stages of increased neuron or astrocyte production (Ishii et al., 2007). Deletion of the N-glycan branching enzyme MGAT1 results in failed neural tube closure and embryonic lethality (Ioffe and Stanley, 1994). Loss of MGAT2 critical for the formation of branched N-glycans causes congenital disease with mental and psychomotor retardation (Schachter, 2001). The role of branched N-glycans in NSPC differentiation warrants further study.

The effects of highly branched N-glycans on NSPCs could relate to N-glycan interactions with galectins. Galectin affinity is proportional to the number of sugar residues available for binding, and so is increased when glycans are more branched and elongated from each branchpoint with N-acetyllactosamine (Lau et al., 2007; Nabi et al., 2015). Galectins may influence NSPC differentiation since NSPCs make galectin 1 (Figure 2), which induces astrocyte maturation *in vitro* (Sasaki et al., 2004) and downregulates neurogenesis in the adult rodent hippocampus (Imaizumi et al., 2011). Interaction of galectin 1 with the highly branched N-glycans induced by GlcNAc may be part of the process leading to more astrocytes but fewer neurons from GlcNAc-treated E12 NSPCs.

N-linked glycosylation regulates multiple receptor classes and is thus well poised to affect cell differentiation.

N-Glycan content governs plasma membrane receptor cell surface residence time and ligand affinity, affecting integrins that bind ECM (β1, α3, α5, and αV), cell-cell adhesion proteins (cadherins), and receptors for growth factors and morphogens (e.g., EGFR, PDGFR, gp130 subunit of CNTFR) (Pinho and Reis, 2015). The loss of MGAT5 and branching reduces cell responses to EGF, PDGF, bFGF, and IGF (Partridge et al., 2004). N-Glycan branching governs cell proliferation through the regulation of growth-promoting (e.g., EGFR and PDGFR) and growth arrest receptors (e.g., TGF-βR) that differ in numbers of N-glycan sites (Lau et al., 2007). Thus, differences in the cell surface glycosylation of neuron- and astrocyte-biased NSPCs may not only contribute to their distinct membrane capacitance values but also specifically regulate multiple types of receptors that guide fate.

Our data suggest that MGAT5 may be more active in cells that will form astrocytes and MGAT3 in neuron-biased NSPCs, raising the possibility that the balance of these enzymes affects fate decisions. MGAT3 antagonizes the activity of MGAT5 since the formation of a bisecting N-glycan by MGAT3 prevents further branching by MGAT5 (Brockhausen et al., 1988). The *Mgat5* gene is more highly expressed in astrogenic-biased NSPCs (E16 and DEP enriched), while the levels of *Mgat3* are higher in more neurogenic NSPC populations (E12 and unsorted) (Figures 1 and 2). GlcNAc treatment increases highly branched N-glycans formed by MGAT5, leading to greater astrogenesis and reduced neurogenesis (Figures 5 and 6). Pluripotent stem cells that differentiate into neurons upregulate MGAT3 expression and have higher cell surface bisecting N-glycans, whereas differentiated astrocytes retain low levels of bisecting N-glycans (Terashima et al., 2014). The balance of MGAT3 and MGAT5 activity regulates several proteins impacting cell function. Overexpression of MGAT5 or loss of MGAT3 induces greater integrin-mediated migration, while high levels of MGAT3 cause reduced migration (Zhao et al., 2006). The generation of more bisecting N-glycans on cadherins fosters greater cell-cell adhesion, whereas more highly branched N-glycans decrease cell-cell adhesion (Guo et al., 2003; Pinho et al., 2009). The degree of MGAT3 and MGAT5-modified N-glycans on the cell surface of NSPCs could regulate responses to a variety of extracellular cues and thus alter fate potential.

EXPERIMENTAL PROCEDURES

NSPC Cell Culture and GlcNAc Treatment

All studies were approved by the Institutional Animal Care and Use Committee at UCI. Mouse E12 or E16 NSPCs were isolated from the cerebral cortex, grown and differentiated as previously described (Lu et al., 2012). GlcNAc (Fisher Scientific) was prepared as a stock solution in medium and supplemented in medium daily. Full details for all experimental procedures are provided in Supplemental Experimental Procedures.

Immunocytochemistry and Fate Potential Analysis

NSPCs were fixed and stained with antibodies as described previously (Nourse et al., 2014). Cells double-positive for MAP2/DCX or MAP2/TUJ1 with neurites at least three times the length of the soma were counted as neurons. Cells expressing GFAP in a filamentous cytoskeletal pattern were counted as astrocytes.

RNA Isolation, RNA Sequencing, and Analysis

RNA was isolated from E12 NSPCs, E16 NSPCs, or E12 cerebral cortex as a control, and cDNA synthesized using M-MLV reverse transcriptase. cDNA was analyzed using the RT^2 Profiler PCR Array (QIAGEN) for 84 mouse glycosylation-related genes or qRT-PCR with primers for specific glycosylation enzymes.

Lectin Flow Cytometry

Live NSPCs were labeled with lectins (e.g., 20 μg/mL FITC-conjugated L-PHA) (Vector Labs) and propidium iodide was used to exclude non-viable cells for analysis.

DEP-Based NSPC Sorting and Capacitance Measurements

Mouse NSPCs were sorted using DEP devices and sorting parameters as described previously, ensuring DEP had no effect on NSPC survival, proliferation, or differentiation potential (Lu et al., 2012; Simon et al., 2014). Dissociated cells (3×10^6 cells/mL) were placed in DEP wells, electrodes were actuated at 100 kHz, 3 Vpp for 5 min or less, and cells attracted to the electrodes were collected. Membrane capacitance measurements used the DEP-Well system (Labeed et al., 2011).

Brain Tissue Section Analysis

CD-1 mice brains were collected at E10, E12, E16, and E18, and sagittal sections (20 μm) stained with antibodies or lectins. Quantitative analysis used ImageJ to calculate signal intensity in at least ten randomly selected areas within each layer (lectin-stained blood vessels were excluded). Minimum intensity values were subtracted from maximum values to control for variation in staining across samples.

Statistical Analysis

Statistical analysis used Prism v.6 software (GraphPad). Comparison of two samples utilized two-tailed unpaired Student's t tests except for qRT-PCR data obtained from E12 NSPCs and sorted cells, which were analyzed by a paired t test since the same sample was measured before and after sorting. Datasets containing more than two samples were analyzed by one-way ANOVA. A Dunnett's *post hoc* correction was applied for the GlcNAc dose-response experiments to compare all GlcNAc treatment groups with the untreated control, and a Tukey's *post hoc* correction was applied for all other multiple comparisons.

SUPPLEMENTAL INFORMATION

Supplemental Information includes Supplemental Experimental Procedures, seven figures, and four tables and can be found with this article online at https://doi.org/10.1016/j.stemcr.2018.08.011.

AUTHOR CONTRIBUTIONS

L.A.F., A.R.Y., and J.L.N. conceived and designed the experiments. A.R.Y., J.L.N., K.R.L., S.N.A., J.A., A.Y.L.J., and L.P.McD. performed the experiments. A.R.Y., J.L.N., K.R.L., S.N.A., J.A., and G.A.B. analyzed the data. A.P.L., E.S.M., and M.D. provided expert advice. A.R.Y., J.L.N., and L.A.F. wrote the manuscript. L.A.F. supervised, supported the study, and finalized the manuscript.

ACKNOWLEDGMENTS

This work was supported in part by NSF CAREER Award IOS-1254060 (to L.A.F.), NIH NINDS T32 NS082174 (predoctoral fellowship to A.R.Y.), CIRM RT1-01074 (to L.A.F.) and CIRM Bridges to Stem Cell Research at California State University, Fullerton TB-01181 (to S.N.A.), NIH NCRR and NCATS through grant UL1 TR001414 (pilot grant to L.A.F.), a Collaborative Multiple Sclerosis (MS) Research Center Award from the National MS Society (to M.D.), the Sue & Bill Gross Stem Cell Research Center at University of California, Irvine, and a gift by Pearl Tze Hosfiel and Keith Hosfiel.

Received: May 2, 2017
Revised: August 10, 2018
Accepted: August 11, 2018
Published: September 6, 2018

REFERENCES

Bagnaninchi, P.O., and Drummond, N. (2011). Real-time label-free monitoring of adipose-derived stem cell differentiation with electric cell-substrate impedance sensing. Proc. Natl. Acad. Sci. USA *108*, 6462–6467.

Brockhausen, I., Narasimhan, S., and Schachter, H. (1988). The biosynthesis of highly branched N-glycans – studies on the sequential pathway and functional role of N-acetylglucosaminyltransferases I, II, III, IV, V and VI. Biochimie *70*, 1521–1533.

Burt, J.P., Pethig, R., Gascoyne, P.R., and Becker, F.F. (1990). Dielectrophoretic characterisation of Friend murine erythroleukaemic cells as a measure of induced differentiation. Biochim. Biophys. Acta *1034*, 93–101.

Cao, Q., Benton, R.L., and Whittemore, S.R. (2002). Stem cell repair of central nervous system injury. J. Neurosci. Res. *68*, 501–510.

Chaboub, L.S., Manalo, J.M., Lee, H.K., Glasgow, S.M., Chen, F., Kawasaki, Y., Akiyama, T., Kuo, C.T., Creighton, C.J., Mohila, C.A., and Deneen, B. (2016). Temporal profiling of astrocyte precursors reveals parallel roles for Asef during development and after injury. J. Neurosci. *36*, 11904–11917.

Cummings, R.D., and Kornfeld, S. (1982). Characterization of the structural determinants required for the high affinity interaction of asparagine-linked oligosaccharides with immobilized *Phaseolus vulgaris* leukoagglutinating and erythroagglutinating lectins. J. Biol. Chem. *257*, 11230–11234.

Desai, S., Vahey, M., and Voldman, J. (2009). Electrically addressable vesicles: tools for dielectrophoresis metrology. Langmuir *25*, 3867–3875.

Flanagan, L.A., Lu, J., Wang, L., Marchenko, S.A., Jeon, N.L., Lee, A.P., and Monuki, E.S. (2008). Unique dielectric properties distinguish stem cells and their differentiated progeny. Stem Cells *26*, 656–665.

Flaris, N., Shindler, K., Kotzbauer, P., Chand, P., Ludwig, C., Konstantinidou, A., and Roth, K. (1995). Developmentally-regulated lectin binding in the embryonic mouse telencephalon. Brain Res. *678*, 99–109.

Garner, O.B., and Baum, L.G. (2008). Galectin-glycan lattices regulate cell-surface glycoprotein organization and signalling. Biochem. Soc. Trans. *36*, 1472–1477.

Gheorghiu, E. (1993). The resting potential in relation to the equivalent complex permittivity of a spherical cell suspension. Phys. Med. Biol. *38*, 979–988.

Guo, H., Lee, I., Kamar, M., and Pierce, M. (2003). N-Acetylglucosaminyltransferase V expression levels regulate cadherin-associated homotypic cell-cell adhesion and intracellular signaling pathways. J. Biol. Chem. *278*, 52412–52424.

Haltiwanger, R.S., and Lowe, J.B. (2004). Role of glycosylation in development. Annu. Rev. Biochem. *73*, 491–537.

Hamouda, H., Ullah, M., Berger, M., Sittinger, M., Tauber, R., Ringe, J., and Blanchard, V. (2013). N-Glycosylation profile of undifferentiated and adipogenically differentiated human bone marrow mesenchymal stem cells: towards a next generation of stem cell markers. Stem Cells Dev. *22*, 3100–3113.

Hartfuss, E., Galli, R., Heins, N., and Götz, M. (2001). Characterization of CNS precursor subtypes and radial glia. Dev. Biol. *229*, 15–30.

He, W., Ingraham, C., Rising, L., Goderie, S., and Temple, S. (2001). Multipotent stem cells from the mouse basal forebrain contribute GABAergic neurons and oligodendrocytes to the cerebral cortex during embryogenesis. J. Neurosci. *21*, 8854–8862.

Heiskanen, A., Hirvonen, T., Salo, H., Impola, U., Olonen, A., Laitinen, A., Tiitinen, S., Natunen, S., Aitio, O., Miller-Podraza, H., et al. (2009). Glycomics of bone marrow-derived mesenchymal stem cells can be used to evaluate their cellular differentiation stage. Glycoconj. J. *26*, 367–384.

Hirota, Y., and Hakoda, M. (2011). Relationship between dielectric characteristic by DEP levitation and differentiation activity for stem cells. Key Eng. Mater. *459*, 84–91.

Imaizumi, Y., Sakaguchi, M., Morishita, T., Ito, M., Poirier, F., Sawamoto, K., and Okano, H. (2011). Galectin-1 is expressed in early-type neural progenitor cells and down-regulates neurogenesis in the adult hippocampus. Mol. Brain *4*, 7.

Ioffe, E., and Stanley, P. (1994). Mice lacking N-acetylglucosaminyltransferase I activity die at mid-gestation, revealing an essential role for complex or hybrid N-linked carbohydrates. Proc. Natl. Acad. Sci. USA *91*, 728–732.

Ishii, A., Ikeda, T., Hitoshi, S., Fujimoto, I., Torii, T., Sakuma, K., Nakakita, S., Hase, S., and Ikenaka, K. (2007). Developmental changes

in the expression of glycogenes and the content of N-glycans in the mouse cerebral cortex. Glycobiology *17*, 261–276.

Labeed, F.H., Lu, J., Mulhall, H.J., Marchenko, S.A., Hoettges, K.F., Estrada, L.C., Lee, A.P., Hughes, M.P., and Flanagan, L.A. (2011). Biophysical characteristics reveal neural stem cell differentiation potential. PLoS One *6*, e25458.

Lau, K.S., Partridge, E.A., Grigorian, A., Silvescu, C.I., Reinhold, V.N., Demetriou, M., and Dennis, J.W. (2007). Complex N-glycan number and degree of branching cooperate to regulate cell proliferation and differentiation. Cell *129*, 123–134.

Lee, A.P., Aghaamoo, M., Adams, T.N.G., and Flanagan, L.A. (2018). It's electric: when technology gives a boost to stem cell science. Curr. Stem Cell Rep. *4*, 116–126.

Lu, J., Barrios, C.A., Dickson, A.R., Nourse, J.L., Lee, A.P., and Flanagan, L.A. (2012). Advancing practical usage of microtechnology: a study of the functional consequences of dielectrophoresis on neural stem cells. Integr. Biol. *4*, 1223–1236.

Males, A., Raich, L., Williams, S.J., Rovira, C., and Davies, G.J. (2017). Conformational analysis of the mannosidase inhibitor kifunensine: a quantum mechanical and structural approach. Chembiochem *18*, 1496–1501.

Muratore, M., Srsen, V., Waterfall, M., Downes, A., and Pethig, R. (2012). Biomarker-free dielectrophoretic sorting of differentiating myoblast multipotent progenitor cells and their membrane analysis by Raman spectroscopy. Biomicrofluidics *6*, 034113.

Nabi, I.R., Shankar, J., and Dennis, J.W. (2015). The galectin lattice at a glance. J. Cell Sci. *128*, 2213–2219.

Nourse, J.L., Prieto, J.L., Dickson, A.R., Lu, J., Pathak, M.M., Tombola, F., Demetriou, M., Lee, A.P., and Flanagan, L.A. (2014). Membrane biophysics define neuron and astrocyte progenitors in the neural lineage. Stem Cells *32*, 706–716.

Partridge, E.A., Le Roy, C., Di Guglielmo, G.M., Pawling, J., Cheung, P., Granovsky, M., Nabi, I.R., Wrana, J.L., and Dennis, J.W. (2004). Regulation of cytokine receptors by Golgi N-glycan processing and endocytosis. Science *306*, 120–124.

Paszek, M.J., DuFort, C.C., Rossier, O., Bainer, R., Mouw, J.K., Godula, K., Hudak, J.E., Lakins, J.N., Wijekoon, A.C., Cassereau, L., et al. (2014). The cancer glycocalyx mechanically primes integrin-mediated growth and survival. Nature *511*, 319–325.

Pinho, S., Reis, C., Paredes, J., Magalhaes, A., Ferreira, A., Figueiredo, J., Wen, X., Carneiro, F., Gartner, F., and Seruca, R. (2009). The role of N-acetylglucosaminyltransferase III and V in the post-transcriptional modifications of E-cadherin. Hum. Mol. Genet. *18*, 2599–2608.

Pinho, S.S., and Reis, C.A. (2015). Glycosylation in cancer: mechanisms and clinical implications. Nat. Rev. Cancer *15*, 540–555.

Prieto, J.L., Lu, J., Nourse, J.L., Flanagan, L.A., and Lee, A.P. (2012). Frequency discretization in dielectrophoretic assisted cell sorting arrays to isolate neural cells. Lab Chip *12*, 2182–2189.

Qian, X., Shen, Q., Goderie, S.K., He, W., Capela, A., Davis, A.A., and Temple, S. (2000). Timing of CNS cell generation: a programmed sequence of neuron and glial cell production from isolated murine cortical stem cells. Neuron *28*, 69–80.

Sasaki, T., Hirabayashi, J., Manya, H., Kasai, K., and Endo, T. (2004). Galectin-1 induces astrocyte differentiation, which leads to production of brain-derived neurotrophic factor. Glycobiology *14*, 357–363.

Schachter, H. (2001). Congenital disorders involving defective N-glycosylation of proteins. Cell Mol. Life Sci. *58*, 1085–1104.

Simon, M.G., Li, Y., Arulmoli, J., McDonnell, L.P., Akil, A., Nourse, J.L., Lee, A.P., and Flanagan, L.A. (2014). Increasing label-free stem cell sorting capacity to reach transplantation-scale throughput. Biomicrofluidics *8*, 064106.

Stoneman, M., Chaturvedi, A., Jansma, D., Kosempa, M., Zeng, C., and Raicu, V. (2007). Protein influence on the plasma membrane dielectric properties: in vivo study utilizing dielectric spectroscopy and fluorescence microscopy. Bioelectrochemistry *70*, 542–550.

Su, Y., Warren, C., Guerrant, R., and Swami, N. (2014). Dielectrophoretic monitoring and interstrain separation of intact clostridium difficile based on their S(surface)-layers. Anal. Chem. *86*, 10855–10863.

Sun, Y., Goderie, S.K., and Temple, S. (2005). Asymmetric distribution of EGFR receptor during mitosis generates diverse CNS progenitor cells. Neuron *45*, 873–886.

Terashima, M., Amano, M., Onodera, T., Nishimura, S., and Iwasaki, N. (2014). Quantitative glycomics monitoring of induced pluripotent- and embryonic stem cells during neuronal differentiation. Stem Cell Res. *13*, 454–464.

Wang, X., Huang, Y., Gascoyne, P., Becker, F., Holzel, R., and Pethig, R. (1994). Changes in friend murine erythroleukemia cell membranes during induced differentiation determined by electrorotation. Biochim. Biophys. Acta *1193*, 330–344.

Zhao, F.T., Li, J., Shi, G.X., Liu, Y., and Zhu, L.P. (2002). Modification of glycosylation reduces microvilli on rat liver epithelial cells. Cell Biol. Int. *26*, 627–633.

Zhao, Y., Nakagawa, T., Itoh, S., Inamori, K., Isaji, T., Kariya, Y., Kondo, A., Miyoshi, E., Miyazaki, K., Kawasaki, N., et al. (2006). N-Acetylglucosaminyltransferase III antagonizes the effect of N-acetylglucosaminyltransferase V on alpha 3 beta 1 integrin-mediated cell migration. J. Biol. Chem. *281*, 32122–32130.

Zhao, Y.Y., Takahashi, M., Gu, J.G., Miyoshi, E., Matsumoto, A., Kitazume, S., and Taniguchi, N. (2008). Functional roles of N-glycans in cell signaling and cell adhesion in cancer. Cancer Sci. *99*, 1304–1310.

Zimmermann, D., Zhou, A., Kiesel, M., Feldbauer, K., Terpitz, U., Haase, W., Schneider-Hohendorf, T., Bamberg, E., and Sukhorukov, V.L. (2008). Effects on capacitance by overexpression of membrane proteins. Biochem. Biophys. Res. Commun. *369*, 1022–1026.

Stem Cell Reports, Volume *11*

Supplemental Information

Cell Surface N-Glycans Influence Electrophysiological Properties and Fate Potential of Neural Stem Cells

Andrew R. Yale, Jamison L. Nourse, Kayla R. Lee, Syed N. Ahmed, Janahan Arulmoli, Alan Y.L. Jiang, Lisa P. McDonnell, Giovanni A. Botten, Abraham P. Lee, Edwin S. Monuki, Michael Demetriou, and Lisa A. Flanagan

Supplemental Figures

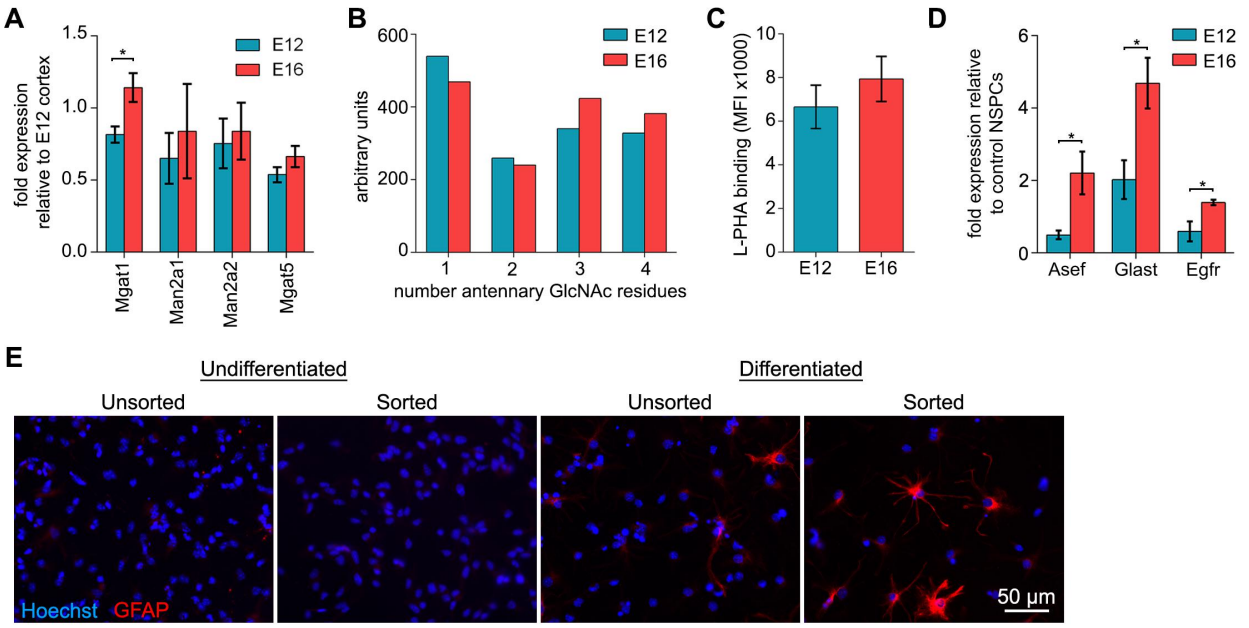

Figure S1. Analysis of E12, E16, and sorted astrocyte-biased NSPCs. Related to Figures 1 and 2. (A) Analysis of N-glycan branching enzyme gene expression by qRT-PCR indicates higher levels of expression in E16 compared to E12 NSPCs (*Mgat1*, p=0.015, unpaired Student's t-test). Values for E12 and E16 NSPCs are relative to E12 cortex (see Supplemental Experimental Procedures). (B) Plasma membrane N-glycans of E12 and E16 NSPCs analyzed by MALDI-TOF mass spectrometry reveal differences in numbers of GlcNAc residues attached to the trimannosyl core (referred to here as branches). One branch corresponds to mono-antennary GlcNAc structures and 2 branches to bi-antennary structures. Three branches correspond to either tri-antennary structures or bi-antennary sugars also containing a bisected GlcNAc. Four branches correspond to either tetra-antennary structures or tri-antennary sugars also containing a bisected GlcNAc. E12 NSPCs contain more 1 or 2 branched N-glycans while E16 NSPCs have more with 3 or 4 branches (n=1). (C) Flow cytometry analysis with lectin L-PHA to detect cell surface highly branched N-glycans indicates similar levels of these structures on E12 and E16 NSPCs, with a trend toward higher levels on E16 cells. Data is represented as mean fluorescence intensity (MFI). (D) Analysis of astrocyte progenitor marker expression by qRT-PCR indicates higher levels of expression in E16 compared to E12 NSPCs (*Asef*, p=0.0300; *Glast*, p=0.0234; *Egfr*, p=0.0311; unpaired Student's t-test). Values for E12 and E16 NSPCs are relative to an independent E12 NSPC sample. (E) Unsorted and DEP-sorted E12 NSPCs were immunostained for GFAP. No GFAP expression was observed in undifferentiated unsorted controls or sorted cells. More GFAP-positive cells were observed in the differentiated sorted sample compared to control NSPCs. Images of differentiated GFAP-labeled cells are identical to those in Figure 2E. All error bars represent standard error of the mean. N=3 or more independent biological repeats unless otherwise noted, (*p<0.05).

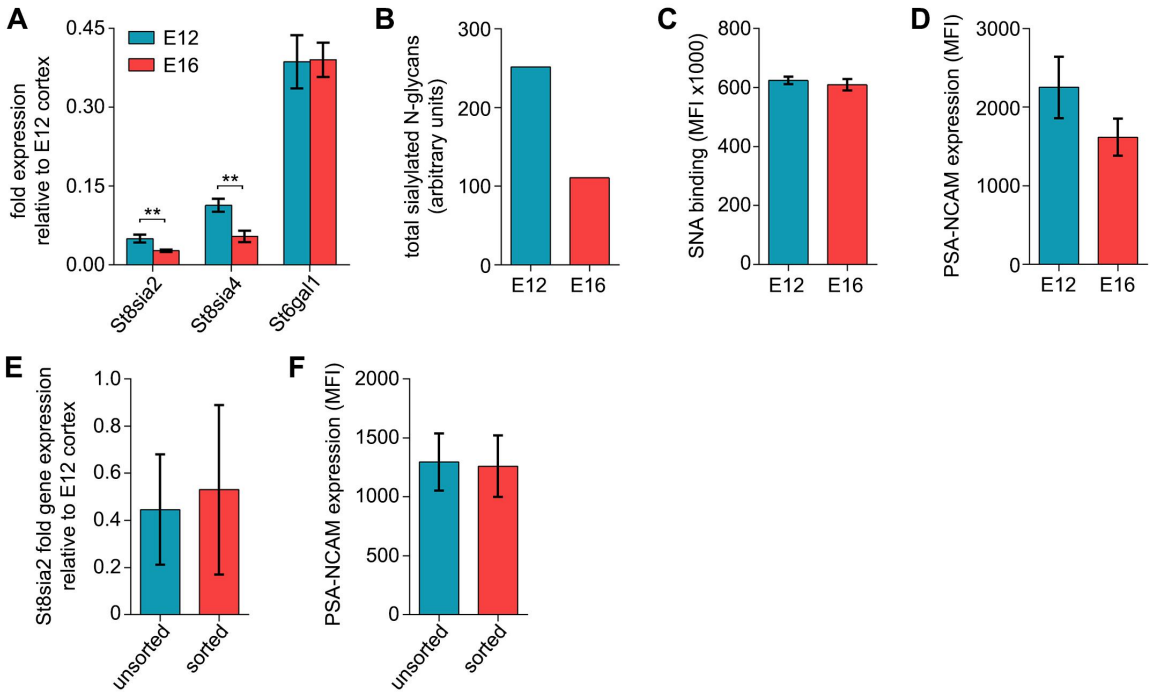

Figure S2. Characterization of NSPC sialic acid. Related to Figures 1 and 2. (A) qRT-PCR gene expression analysis of transcripts encoding sialic acid modifying enzymes indicates higher expression of *St8sia2* and *St8sia4* in E12 compared to E16 NSPCs (*St8sia2*, p=0.007, *St8sia4*, p=0.0072, unpaired Student's t-test). There was no difference in *St6gal1* expression between the two cell populations. Values for E12 and E16 NSPCs are relative to those of E12 cortex. (B) Analysis of plasma membrane N-glycans from E12 and E16 NSPCs by MALDI-TOF mass spectrometry shows more sialic acid modified N-glycans on E12 than E16 NSPCs (n=1). (C) Flow cytometry analysis with lectin SNA to detect cell surface sialic acid containing N-glycans modified by ST6GAL1 indicates similar levels of these structures on E12 and E16 NSPCs. Data is represented as mean fluorescence intensity (MFI). (D) Flow cytometry analysis of PSA-NCAM indicates a non-significant lower (p=0.0891) expression of PSA-NCAM on E16 NSPCs compared to E12 NSPCs. Data represented as MFI. (E) Expression of the sialic acid modifying enzyme *St8sia2* analyzed by qRT-PCR indicates similar levels in control and sorted astrocyte-biased NSPCs. Values for E12 NSPCs and sorted cells are relative to those of E12 cortex. (F) Flow cytometry analysis of PSA-NCAM indicates similar levels between control and sorted cells. All error bars represent standard error of the mean. N=3 or more independent biological repeats unless otherwise noted, (**p<0.01).

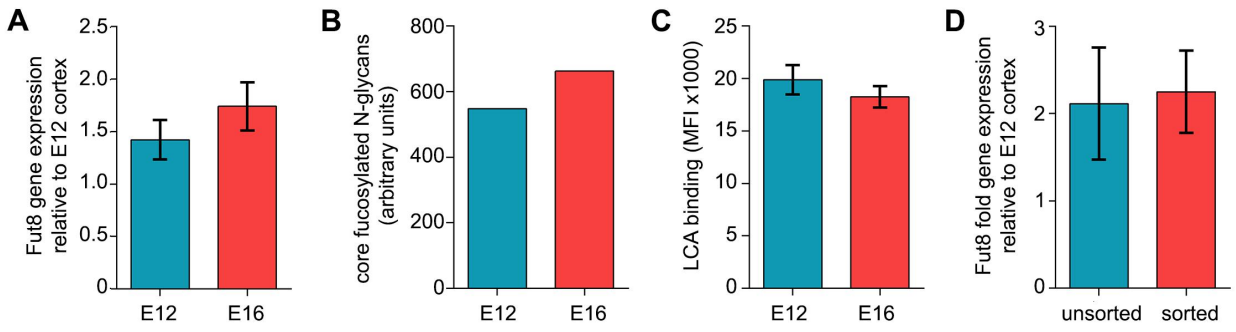

Figure S3. Characterization of NSPC core fucose glycosylation. Related to Figures 1 and 2. (A) qRT-PCR gene expression analysis of transcripts encoding the *Fut8* enzyme that adds core fucose indicates similar levels in E12 and E16 NSPCs. Values for E12 and E16 NSPCs are relative to those of E12 cortex. (B) Plasma membrane N-glycans of E12 and E16 NSPCs analyzed by MALDI-TOF mass spectrometry show similar amounts of core fucose modified N-glycans on E12 and E16 NSPCs (n=1). (C) Flow cytometry analysis with lectin LCA to detect cell surface core fucose containing N-glycans indicates similar levels of these structures on E12 and E16 NSPCs. Data is represented as mean fluorescence intensity (MFI). (D) Expression of *Fut8* analyzed by qRT-PCR indicates similar levels in control and sorted E12 NSPCs. Values for E12 NSPCs and sorted cells are relative to those of E12 cortex. All error bars represent standard error of the mean. N=3 or more independent biological repeats unless otherwise noted.

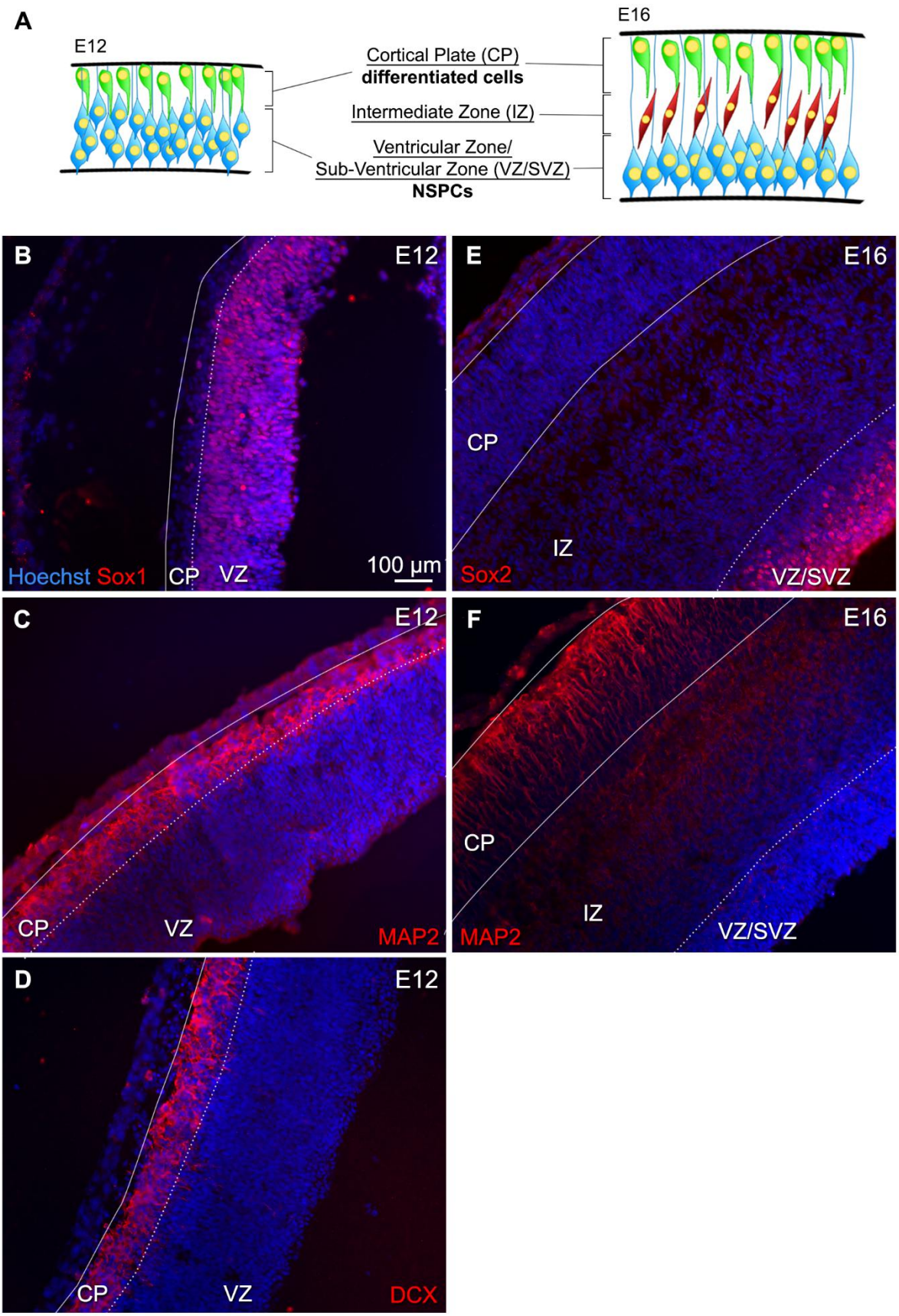
A
E12
E16
Cortical Plate (CP)
differentiated cells
Intermediate Zone (IZ)
Ventricular Zone/
Sub-Ventricular Zone (VZ/SVZ)
NSPCs
B
E12
Hoechst Sox1
CP
VZ
100 µm
E
E16
CP
IZ
Sox2
VZ/SVZ
C
E12
CP
VZ
MAP2
F
E16
CP
IZ
MAP2
VZ/SVZ
D
E12
CP
VZ
DCX

Figure S4. Identification of the VZ/SVZ and CP during embryonic cortical development. Related to Figure 3. **(**A) Schematic representing the layers of the developing cerebral cortex depicts the VZ and CP at E12 and the VZ/SVZ, IZ, and CP at E16. Stem and progenitor cells in the VZ/SVZ are shown in blue, migrating cells in the IZ are in red, and the differentiated cells of the CP are in green. (B) Sagittal sections of the E12 mouse embryonic cortex were stained with antibodies to SOX1 to identify NSPCs and define the borders of the VZ. (C) E12 sagittal sections stained with antibodies to MAP2 to identify differentiated neurons define the borders of the CP. (D) Similarly, DCX antibodies detect differentiated neurons in the E12 CP. (E) Sagittal sections of the E16 mouse embryonic cortex were stained with antibodies to SOX2 to mark the NSPCs of the VZ/SVZ. (F) MAP2 staining of E16 sagittal sections marks the differentiated neurons in the CP; note the intervening IZ between the VZ/SVZ and CP at E16. All cell nuclei were labeled with Hoechst.

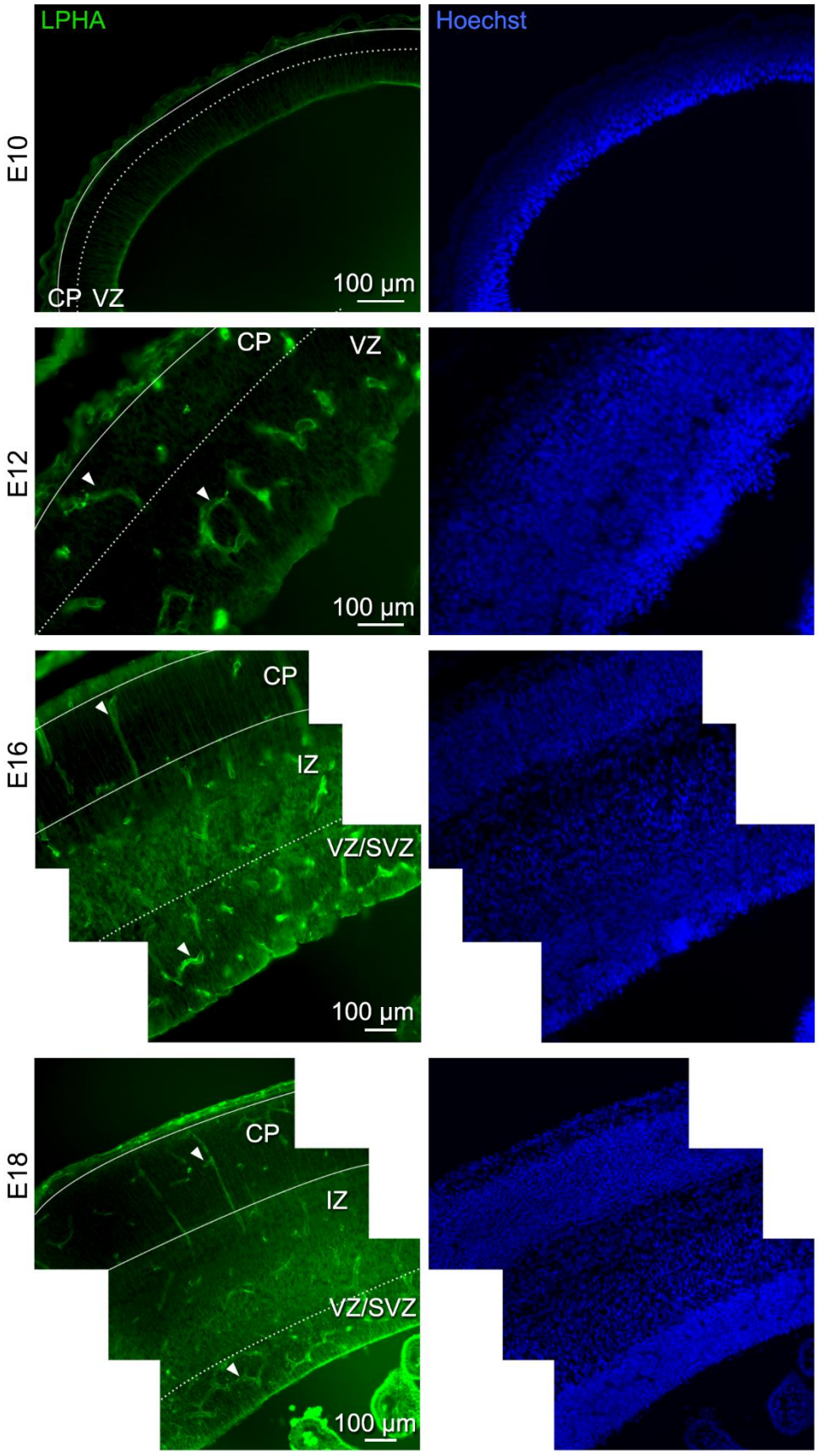
LPHA
Hoechst
E10
CP
VZ
100 μm
E12
CP
VZ
100 μm
E16
CP
IZ
VZ/SVZ
100 μm
E18
CP
IZ
VZ/SVZ
100 μm

Figure S5. Labeling of the E10 to E18 developing cerebral cortex with lectin L-PHA to detect highly branched N-glycans. Related to Figure 3. Lectin L-PHA indicates the presence of highly branched tetra-antennary N-glycans in sagittal sections of the developing embryonic cerebral cortex at E10, E12, E16, and E18. Dotted lines denote the boundaries between the NSPC niches (VZ in E12 and VZ/SVZ in E16) and regions containing more differentiated cells, the cortical plate (CP) and migrating progenitors, intermediate zone (IZ). Solid lines indicate the outer boundaries of the CP and IZ. Arrowheads point to blood vessels, which stain strongly for L-PHA and were excluded from quantitative analysis. More intense L-PHA staining is evident in the E16 and E18 NSPC niche (VZ/SVZ) than the E10 or E12 niche (VZ). Right hand panels are corresponding Hoechst stained nuclei for each panel on the left. Images of E12 and E16 LPHA-stained sections are identical to those in Figure 3A.

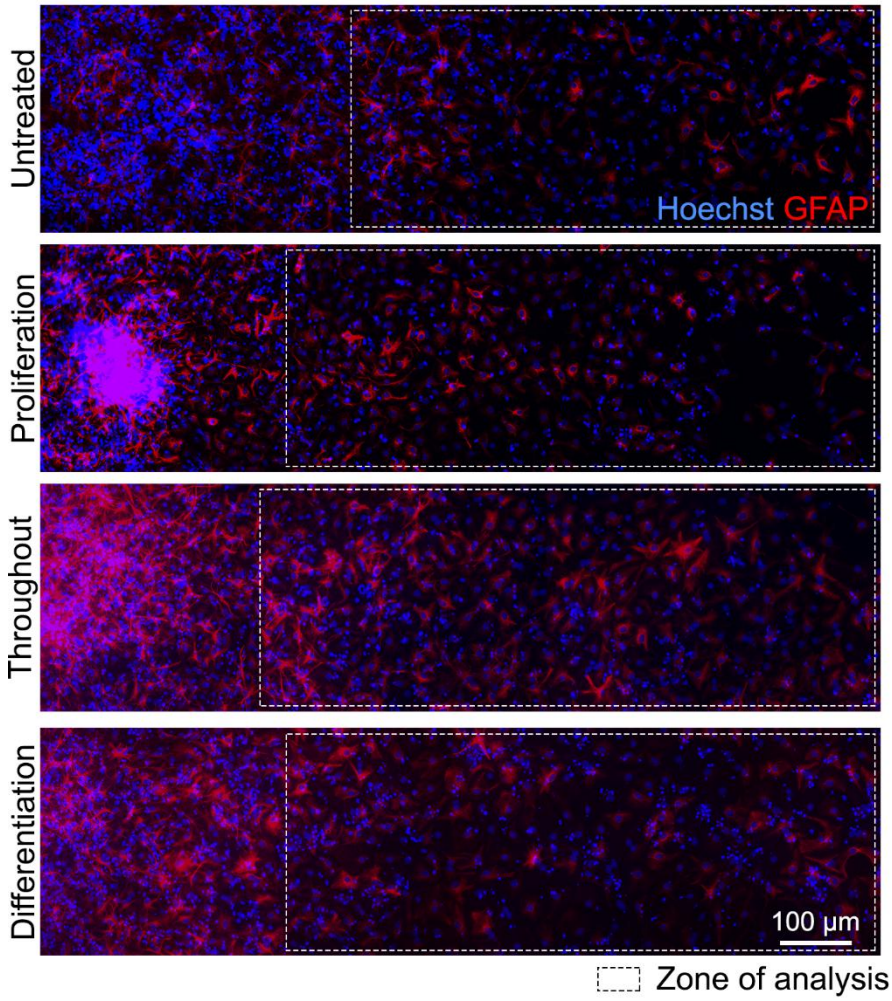

Figure S6. Whole field images of GFAP-positive cells. Related to Figure 6. Images of GFAP-positive astrocytes differentiated from E12 NSPCs indicate the zones of cells used for analysis (dashed boxes) to avoid high cell density regions (left side of each image). Cells were untreated or treated with 80 mM GlcNAc during proliferation, throughout proliferation and differentiation, or during differentiation (see Figure 6A). All cell nuclei were labeled with Hoechst.

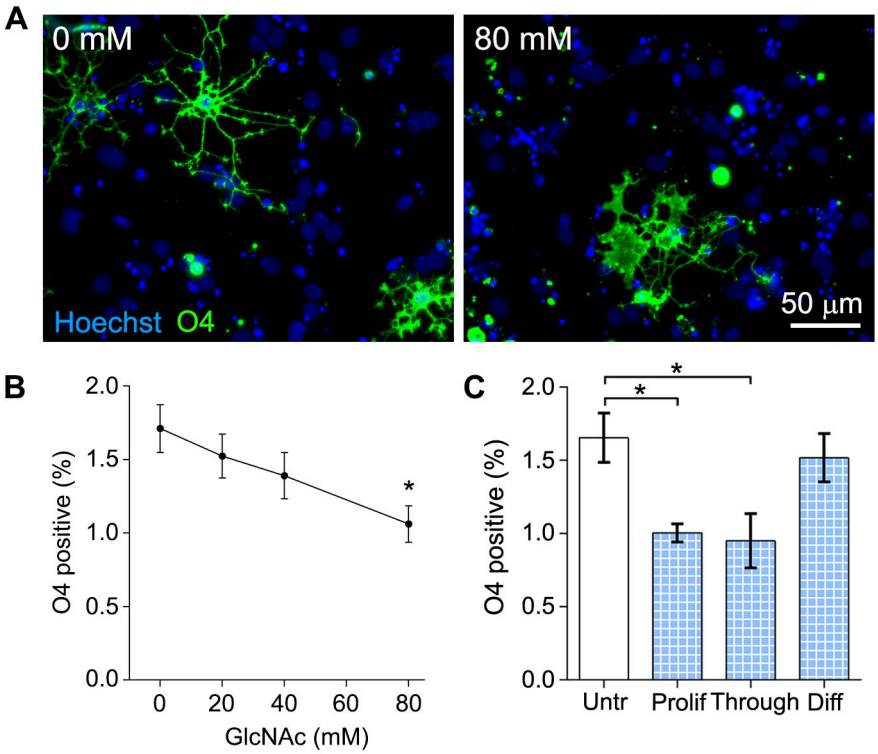

Figure S7. GlcNAc treatment decreases oligodendrocyte formation from E12 mouse NSPCs. Related to Figure 6. (A) E12 NSPCs treated with 80 mM GlcNAc during 3 days as undifferentiated cells and for an additional 7 days during differentiation generated fewer oligodendrocytes stained with O4 (green) than control NSPCs (0 mM, untreated). Some non-specific globular signal was present in all samples and was excluded from analysis. All nuclei were labeled with Hoechst (blue). (B) The percentage of O4-positive oligodendrocytes formed from E12 NSPCs decreases with increasing GlcNAc concentration (one-way ANOVA, p=0.0222). *Post hoc* analysis by Dunnett's test indicates significant decrease in oligodendrocyte formation after supplementation with 80 mM GlcNAc (p=0.0161) compared to untreated E12 NSPCs. (C) E12 NSPCs were treated with 80 mM GlcNAc in the proliferation stage (Prolif, 3 days), throughout both proliferation and differentiation stages (Through, 10 days), or during the differentiation stage (Diff, 7 days). The percentage of O4 positive oligodendrocytes was significantly decreased when NSPCs were treated with GlcNAc during the proliferation stage or throughout both stages (Untr v Prolif p=0.0383, Untr v Through p=0.0144, one-way ANOVA, Tukey *post hoc* for multiple comparisons) but not the differentiation stage, suggesting an effect on undifferentiated NSPCs but not differentiated cells. All error bars represent standard error of the mean. N=3 or more independent biological repeats, (*p<0.05).

Supplemental Tables

Table S1: **N-glycosylation enzymes of E12 and E16 NSPCs. Related to Figure 1**. Bolded enzymes show expression difference greater than 1.2-fold.

Enzyme	E16 fold over E12	Function
Man2a2	**1.6935**	**Removes mannose from N-glycans to initiate complex branching**
Fut8	**1.5476**	**Adds α1-6 linked fucose to first GlcNAc on N-glycan core**
B3gnt2	**1.5476**	**Involved in the formation of poly-N-acetyllactosamine**
St6gal1	**1.5263**	**Adds α2-6 linked sialic acid to galactose residues**
Man2a1	**1.2924**	**Removes mannose from N-glycans to initiate complex branching**
B4galt5	**1.2483**	**Adds galactose to N-glycans**
Mgat5	**1.2142**	**Adds β1-6 linked GlcNAc on highly-branched N-gycans**
Prkcsh	1.1810	B-subunit of glucosidase II
Mgat1	1.1567	Adds first β1-2 linked GlcNAc to form hybrid and complex N-glycans
Ganab	1.1408	A-subunit of glucosidase II; cleaves glucose from immature N-glycans in the ER
B4galt1	1.0000	Adds galactose to GlcNAc residues on branched N-glycans
St3gal2	1.0000	Adds α2-3 linked sialic acid to galactose
B3gnt4	0.9931	Biosynthesis of poly-N-acetyllactosamine
Mgat2	0.9794	Adds second β1-2 linked GlcNAc to form di-antennary N-glycans
Man1b1	0.9659	Removes mannose from N-glycans
B4galt3	0.9461	Adds first galactose for poly-N-acetyllactosamine chains
Man1a2	0.9395	Removes mannose from N-glycans necessary to initiate biosynthesis of branched N-glycans
Mogs	0.9013	Cleaves glucose from mannose in early N-glycan processing
Mgat4b	0.8888	Adds β1-4 linked GlcNAc on highly-branched N-gycans
Mgat4a	0.8526	Adds β1-4 linked GlcNAc on highly-branched N-gycans
Man1c1	0.8011	Removes mannose from N-glycans
Fut11	**0.7792**	**α1-3 fucosyltransferase**
B4galt2	**0.7423**	**Involved in the formation of poly-N-acetyllactosamine**
St8sia4	**0.5664**	**Also known as PST, biosynthesis of polysialic acid**
Mgat3	**0.5471**	**Adds β1-4 linked GlcNAc to form bisected N-glycans**
St8sia2	**0.2755**	**Also known as STX, biosynthesis of polysialic acid**
B3gnt8	low expr	Elongates branched N-glycans, strong activity toward tetra-antennary N-glycans
Man1a	low expr	Removes mannose from N-glycans necessary to initiate biosynthesis of branched N-glycans
Mgat4c	low expr	Adds β1-4 linked GlcNAc on highly-branched N-gycans
St8sia3	low expr	Biosynthesis of polysialic acid
B3gnt3	not expr	Involved in the formation of poly-N-acetyllactosamine
Man2b1	not expr	Removes mannose from N-glycans

Table S2: O-glycosylation enzymes of E12 and E16 NSPCs. Related to Figure 1. Bolded enzymes show expression difference greater than 1.2-fold.

Enzyme	E16 fold over E12	Function or possible function based on homology
Galnt7	**1.74**	**Adds galactose to pre-existing O-linked GalNAc on serine/threonine (S/T) residues**
Galnt4	**1.65**	**Adds initial GalNAc onto S/T in mucin-type O-glycans**
Pofut2	**1.37**	**Generates O-fucosylated proteins**
Pomt1	**1.23**	**Works with Pomt2 to generate O-mannose glycans**
Ogt	1.19	Adds initial GlcNAc to S/T to generate cytoplasmic and nuclear O-GlcNAc glycans
B3glct	1.1567	Transfers glucose to O-linked fucosyl glycans
Pomgnt1	1.07	Adds GlcNAc onto O-mannose glycans
Galnt1	1.06	Adds initial GalNAc onto S/T for mucin type O-glycans
St6GalNAc1	1.0479	Adds sialic acid to galactose residues of O-linked sugars
Pomt2	1	Works with Pomt1 to generate O-mannose glycans
Galnt11	0.97	Initiates biosynthesis of O-linked GalNAc glycans
Galnt2	0.97	Initiates biosynthesis of O-linked GalNAc glycans
C1galt1c1	0.97	Chaperone necessary for C1galt1 and core 1 O-glycan synthesis
C1galt1	0.93	Generates the core 1 O-glycan structure
Galnt10	0.87	Adds initial GalNAc onto S/T for mucin type O-glycans
Pofut1	0.85	Adds initial fucose to S/T to generate O-fucosylated proteins
Wbscr17	0.84	Initiates biosynthesis of O-linked GalNAc glycans
Galnt16	0.81	Adds initial GalNAc onto S/T in mucin-type O-glycans
St3gal1	**0.79**	**Adds sialic acid to galactose residues of O-linked sugars**
Galnt13	**0.68**	**Adds initial GalNAc onto S/T in mucin-type O-glycans**
Mgat5b	**0.48**	**Adds GlcNAc to mannose to generate branched O-mannose glycans**
Galnt12	low expr	Initiates biosynthesis of O-linked GalNAc glycans
Galnt14	low expr	Adds initial GalNAc onto S/T in mucin-type O-glycans
Galnt3	low expr	Adds initial GalNAc onto S/T in mucin-type O-glycans
Galnt9	low expr	Adds initial GalNAc on S/T in mucin-type O-glycans
Gcnt1	low expr	Generates the core 2 O-glycan structure
St8sia6	low expr	Biosynthesis of polysialic acid on O-glycans
A4gnt	low expr	Transfers GlcNAc to core 2 O-glycans to form type III mucins
Galnt5	not expr	Adds initial GalNAc onto S/T in mucin-type O-glycans
Galnt6	not expr	Adds initial GalNAc onto S/T in mucin-type O-glycans
Galntl5	not expr	Adds initial GalNAc onto S/T in mucin-type O-glycans
Galntl6	not expr	Adds initial GalNAc onto S/T in mucin-type O-glycans
Gcnt3	not expr	Involved in biosynthesis of core 2 and core 4 O-glycans of mucins

Table S3: Enzymes of E12 and E16 NSPCs involved in endoplasmic reticulum (ER) quality control, targeting of enzymes to lysosomes, or lysosomal degradation of glycans. Related to Figure 1. Bolded enzymes show expression difference greater than 1.2-fold.

Enzyme	E16 fold over E12	Function
Manba	**1.8921**	**Lysosomal mannosidase**
Hexa	**1.7901**	**A-subunit of lysosomal enzyme that degrades GM2 ganglioside**
Aga	**1.7532**	**Lysosomal enzyme; cleaves GlcNAc-Asn linkage on N-linked glycoproteins**
Fuca1	**1.2924**	**Lysosomal enzyme; degrades fucose containing glycoproteins**
Nagpa	**1.2746**	**Cleaves GlcNAc from mannose; involved in lysosomal enzyme trafficking from Golgi to lysosome**
Uggt1	**1.2142**	**Re-glucosylates N-glycans of misfolded proteins in the ER**
Edem3	1.1567	Participates in ER-associated degradation (ERAD) by cleaving mannose residues from N-glycans
Edem1	1.1408	Participates in ERAD by cleaving mannose residues from N-glycans and targets misfolded glycoproteins for degradation
Uggt2	1.0718	Re-glucosylates N-glycans of misfolded proteins in the ER
Hexb	1.0497	B-subunit of lysosomal enzyme that degrades GM2 ganglioside
Glb1	1.014	Lysosomal enzyme; involved in degradation
Neu3	1.0070	Plasma membrane sialidase
Neu1	0.9862	Lysosomal sialidase
Edem2	0.9461	Participates in ERAD by trimming mannose in the ER
Fuca2	0.9138	Lysosomal enzyme, degrades fucose containing glycoproteins
Gnptg	0.9075	Generates glycans necessary for trafficking lysosomal enzymes to lysosome
Gnptab	0.895	Generates glycans necessary for trafficking lysosomal enzymes to lysosome
Neu4	low expr	Lysosomal sialidase
Neu2	not expr	Cytoplasmic sialidase

Table S4: DNA primers for qRT-PCR. Related to Figure 2 and Supplemental Figure S1.

Gene	Forward Primer (5'→ 3')	Reverse Primer (5' → 3')	Expected length (bp)
Asef (probe 1)	TCTCCAGAGTCTCCGCATCTTC	GTGGCATCCATCACTTCGATG	353
Asef (probe 2)	GAGGAGGTGGAGAGCAACTG	GCGGTAGATGTCCTCGATGTTC	484
Slc1a3 (GLAST)	TTTCTCTCTAGGGGCAGGCT	CAGAAGGGAGGGCCTCTAGT	140
Egfr	TCTTCAAGGATGTGAAGTGTG	TGTACGCTTTCGAACAATGT	145
GAPDH	ATACGGCTACAGCAACAGGG	GCCTCTCTTGCTCAGTGTCC	105

Supplemental Experimental Procedures

NSPC cell culture:

CD-1 mice (Charles River) were purchased, selected randomly, and bred as approved by the University of California, Irvine Institutional Animal Care and Use Committee. Dorsal forebrain cortical tissue was dissected from the cerebral cortices of embryonic day 12.5 (E12) and 16.5 (E16) mice and placed in dissection buffer: PBS, 0.6% glucose, 50 U/mL Pen/Strep. Cortical tissue from multiple embryos within the same litter was pooled, and a subsequent culture from a single litter was considered a biological repeat. The tissue was dissociated using 0.05% Trypsin-EDTA at 37^{o}C for 10 min. Afterward, trypsin was inhibited using soybean trypsin inhibitor (Life Technologies) and dissociated cells were re-suspended in proliferation medium containing DMEM, 1x B27, 1x N2, 1 mM sodium pyruvate, 2 mM L-glutamine, 1 mM N-acetylcysteine, 20 ng/mL EGF, 10 ng/mL bFGF, and 2 µg/mL heparin. Cells were seeded at 150,000 cells/mL into non-tissue culture treated plastic plates and grown as non-adherent spheres. Cell cultures were passaged approximately every 3 days using enzyme-free NeuroCult Chemical Dissociation Kit (Mouse) (StemCell Technologies). All NSPC cultures were passaged at least once prior to experimental use. NSPCs were plated as adherent cultures for differentiation. HCl-washed German glass coverslips (Assistant/Carolina Biological Supply, Burlington, NC) were pretreated with poly-D-lysine (40 µg/mL in milliQ H_20) for 5 minutes then coated with laminin (20 µg/mL in EMEM) at 37^{o}C for 24 hours prior to cell adhesion. Whole neurospheres were seeded onto the laminin-coated coverslips in proliferation medium. After 24 hours, proliferation medium was removed and replaced with differentiation medium (same components as proliferation medium but excluding EGF, bFGF, and heparin) to induce differentiation. NSPCs were differentiated into neurons and astrocytes in these conditions for 3 days and oligodendrocytes for 7 days. For 7 day differentiated samples, culture media was replaced after 3 days.

GlcNAc and Kifunensine treatment of NSPCs:

A stock solution of 800 mM N-acetylglucosamine (GlcNAc, Fisher Scientific) was prepared in proliferation medium. For dose response experiments, the stock solution was added to E12 NSPC cultures in proliferation medium to create final concentrations ranging from 20 to 80 mM GlcNAc and the same concentration of GlcNAc was maintained in the differentiation medium (Grigorian et al., 2007). The medium was re-supplemented with fresh GlcNAc every 24 hours since GlcNAc breaks down over time in aqueous solutions. For some experiments NSPCs were treated with 80 mM GlcNAc for 3 days in proliferation medium then dissociated for analysis. Experiments designed to test the effects of GlcNAc at different stages of cell growth and differentiation used GlcNAc supplementation in either the proliferation medium only (and not the differentiation medium), the differentiation medium only (and not the proliferation medium), or treated throughout proliferation and differentiation so included in both media. When GlcNAc was added to differentiation medium, the GlcNAc stock was also prepared in differentiation medium and GlcNAc was re-supplemented daily in the culture media. Control cells were grown in medium lacking supplementation with GlcNAc. Kifunensine (0.5 µM, Sigma Aldrich) was added to proliferation medium in some experiments to block the incorporation of GlcNAc into highly branched N-glycans. Both kifunensine and GlcNAc were withdrawn during differentiation conditions in these experiments.

Proliferation Assays

Proliferation assays utilized phospho-histone H3 immunostaining or EdU incorporation as previously described (Lu et al., 2012). Cells undergoing mitosis were visualized by immunocytochemistry utilizing the primary antibody mouse anti-phospho-histone H3 (Ser10) (6G3) IgG (Cell Signaling Technology 9706S) and the secondary antibody donkey anti-mouse IgG Alexa Fluor 488 (Thermo Fisher Scientific A21202). All cells were counterstained with Hoechst 33342 nuclear dye (Thermo Fisher Scientific). Cells that passed through at least one S-phase were visualized using EdU incorporation (Click-iT EdU Alexa Fluor 555 Imaging Kit, Thermo Fisher Scientific). Proliferation medium of adherent NSPCs was supplemented with 10 μM EdU and cells incubated at 37^{o} C for 4 hours. Afterwards, cells were fixed and permeabilized as described above. After washing with PBS, cells were incubated with the EdU Click-iT reaction cocktail for 30 min at room temperature in the dark and counterstained with Hoechst 33342 nuclear dye (Thermo Fisher Scientific). Cells were analyzed using manual counting software in ImageJ and positively labeled cells were counted as a percentage of all Hoechst-stained cells in 5 randomly selected fields.

Cell Viability

Cell viability was assessed using the LIVE/DEAD Viability/Cytotoxicity Kit (for mammalian cells) (Thermo Fisher Scientific). Briefly, dissociated E12 NSPCs were re-suspended in 1 mL proliferation medium containing 100 nM calcein-AM to label live cells and 8 μM ethidium homodimer-1 to label dead cells. The cell suspension was incubated for 15-20 min at room temperature, protected from the light. Cell apoptosis was analyzed using the Dead Cell Apoptosis Kit (Thermo Fisher Scientific). Briefly, dissociated E12 NSPCs were re-suspended in the provided 5x Annexin V reaction buffer (50 mM HEPES, 700 mM NaCl, 12.5 mM $CaCl_2$, pH 7.4) containing Alexa Fluor 488-conjugated Annexin V and 1 μg/ml propidium iodide. The cell suspension was incubated for 10 min on ice, protected from the light. Control apoptotic cells were generated by culturing NSPCs at 37ºC in growth medium containing 200 μM H_2O_2 for 3 hours prior to analysis. The cells were analyzed with a BD LSR II flow cytometer, and the data collected using the BD FACSDIVA software. All data analysis was performed using FlowJo v10.1.

Immunocytochemistry and fate potential analysis

After differentiation, adherent cells were fixed with 4% paraformaldehyde (4% paraformaldehyde, 5 mM $MgCl_2$, 10 mM EGTA, 4% sucrose in PBS) for 10 min, and the cell membranes were permeabilized with 0.3% Triton-X 100 in PBS for 5 min. Cells were blocked using 5% BSA in PBS for 1 hour then incubated with the primary antibody for approximately 18 hours at 4^{o} C and the secondary antibody for 2 hours at room temperature in the dark. All cells were counterstained using a Hoechst 33342 nuclear dye (Thermo Fisher Scientific) and coverslips were mounted onto glass slides using VectaShield mounting medium (Vector Labs). Cells were visualized using a Nikon Eclipse Ti-E fluorescence microscope at 20x magnification, and all images were acquired using NIS Elements AR 4.51 image capturing and analysis software. Antibodies for immunostaining included mouse anti-MAP2 IgG (Sigma M9942) at 1:200, goat anti-DCX (C-18) IgG (Santa Cruz Biotechnology SC8066) at 1:200, rabbit-anti TUJ1 IgG (Sigma T2200) at 1:100, mouse anti-O4 IgM (R&D Systems MAB1326) at 1:100, or mouse anti-GFAP IgG (Sigma G9269) at 1:200 with all antibodies prepared in 1% BSA in PBS. Secondary antibodies donkey anti-mouse IgG Alexa Fluor 555, donkey anti-goat IgG Alexa Fluor 555, donkey-anti rabbit IgG Alexa Fluor 555, donkey anti-mouse IgG Alexa Fluor 488, and goat anti-mouse IgM heavy chain Alexa Fluor 555 (Thermo Fisher Scientific A31570, A21432, A21206, A21202, A21426) were diluted 1:200 in 1% BSA.

For fate analysis, at least 3 independent sets of NSPCs derived from 3 different litters were analyzed using manual counting software built into ImageJ. The percentage of cells that differentiated into double-positive MAP2/DCX or MAP2/TUJ1 neurons with neurite lengths of at least 3 times the length of the soma was calculated from 5 randomly selected fields per experiment with more than 1000 cells counted per experimental group in each of the 3 independent experiments, so over 3000 cells per group. The percentages of GFAP-positive astrocytes were calculated from randomly selected fields of cells adjacent to the sphere attachment site but not from the dense cells within the sphere since cell density and cell death affect astrocyte GFAP reactivity. Cells expressing GFAP in a filamentous cytoskeletal pattern were counted as astrocytes and 3000 or more cells per experimental group were analyzed.

RNA isolation, array, and qRT-PCR analysis

NSPC or E12 cerebral cortex total RNA was isolated using the Aurum total RNA isolation kit (Bio-Rad Laboratories), and cDNA was synthesized using M-MLV reverse transcriptase (Promega) in the S100 Thermal

Cycler (Bio-Rad) after which the enzyme was heat inactivated at 95^{o}C for 5 min. cDNA generated from E12 and E16 NSPC total RNA was analyzed using the RT^{2} Profiler PCR Array (Qiagen) for 84 glycosylation-related genes in mouse. Function of glycosylation enzymes is listed in Tables S1, S2, S3(Varki, 2009).

Analysis of glycosylation enzyme expression was performed using TaqMan probe-based gene expression assays with the Taqman universal PCR master mix (Life Technologies 4304437) and commercially available Taqman high specificity probes. Taqman probes used for qRT-PCR analysis included mouse actin (Mm00607939_s1), *18s* (Mm0392899_g1), *Man2a1* (Mm00484781_m1), *Man2a2* (Mm00556618_m1), *Mgat1* (Mm01288784_m1), *Mgat5* (Mm01291751_m1), *Fut8* (Mm00489789_m1), *St6gal1* (Mm00486119_m1), *St8sia2* (Mm0131039_m1), *St8sia4* (Mm01292231_m1) all from Life Technologies. In experiments analyzing astrocyte progenitor marker expression, qRT-PCR was performed using short oligonucleotide DNA primers customized through NCBI's Primer-BLAST (ordered from IDT) (see Table S4) and PowerUp™ SYBR® Green Master Mix (Thermo Fisher Scientific). All qRT-PCR experiments were performed using the ABI Viia7 instrument, and data was exported from the ABI Viia7 software. Data from the PCR arrayTaqman, and SYBR green assays were analyzed by the comparative cycle (C_t) method (Cheng et al., 2006). The PCR array C_t experimental data was normalized to internal array controls. The Taqman assay data utilized 18s or actin to normalize the experimental C_t values. The SYBR green assay used *Gapdh* as the reference gene. Where indicated, gene expression was further normalized to RNA isolated from whole E12 cerebral cortex or *in vitro* NSPC samples as indicated

RNA sequencing and analysis

RNA was isolated from suspended E12 mouse NSPC cultures from three separate litters using the Bio-Rad RNA Isolation Kit (Genicity, Irvine, CA, USA; G00065). Genomic DNA contamination of all RNA samples was assessed by using qRT-PCR for mouse 18S and *Gapdh* with and without reverse transcriptase and found to be insignificant. cDNA for qRT-PCR was synthesized using M-MLV reverse transcriptase (Promega). Total RNA was further monitored for quality control using the Agilent Bioanalyzer Nano RNA chip and Nanodrop absorbance ratios for 260/280nm and 260/230nm.

RNA library preparation and sequencing was performed at the UCI Genomics Core as previously described (Arulmoli et al., 2016). Library construction was performed according to the Illumina TruSeq mRNA stranded protocol. The input quantity for total RNA was 250ng and mRNA was enriched using oligo dT magnetic beads. The enriched mRNA was chemically fragmented for five minutes. First strand synthesis used random primers and reverse transcriptase to make cDNA. After second strand synthesis the double-stranded cDNA was cleaned using AMPure XP beads and the cDNA was end repaired and the 3' ends were adenylated. Illumina barcoded adapters were ligated on the ends and the adapter ligated fragments were enriched by nine cycles of PCR. The resulting libraries were validated by qPCR and sized by Agilent Bioanalyzer DNA high sensitivity chip. The concentrations for the libraries were normalized and the libraries were multiplexed together. The concentration for clustering on the flowcell was 12.5 pM. The multiplexed libraries were sequenced on one lane using single read 100 cycles chemistry for the HiSeq 2500. The version of HiSeq control software was HCS 2.2.58 with real time analysis software, RTA 1.18.64.

For sequence mapping and bioinformatic analysis, RNA-Seq data was processed as described previously (Lissner et al., 2015). All bioinformatics analyses were conducted using the Galaxy platform (Goecks et al., 2010). Reads were aligned to the mouse NCBI37/mm9 reference genome with the TopHat program (Trapnell et al., 2010) using most default parameters. Alignments were restricted to uniquely mapping reads with two possible mismatches permitted. RPKM (reads per kilobase pair per million mapped reads) were calculated as described (Mortazavi et al., 2008) for mm9 RefSeq genes using the SeqMonk program (http://www.bioinformatics.babraham.ac.uk/projects/seqmonk/). mRNA RPKMs were derived by counting exonic reads and dividing by mRNA length.

Membrane preparation and MALDI-TOF Mass Spectroscopy

Approximately 7x10^{7} NSPCs were washed with PBS containing 0.6% glucose twice. Cells were suspended in an ice-chilled hypotonic solution (1x PBS diluted 1:10) containing AEBSF and leupeptin protease inhibitors and lysed by freeze-thaw cycling between a dry ice/ethanol bath and 37^{o}C water bath. The sample was centrifuged at 75 x g for 15 min at 4^{o}C to remove nuclei, large organelles, and unlysed cells. The supernatant was collected and further centrifuged at 100,000 x g for 1 hour at 4^{o}C using a Beckman Ultracentrifuge (rotor TL110). The pellet containing the cell membrane fraction was isolated and sent to the Glycotechnology Core Facility of the Glycobiology Research and Training Center at the University of California, San Diego where MALDI-TOF Mass Spectroscopy

was performed as described by Lee *et al*. (Lee et al., 2007). Glycan species were obtained from E12 and E16 NSPCs and the total intensity measured for each glycan structure was analyzed. N-glycan species formed by core branching glycosylation enzymes were grouped according to the number of branches emanating from the core structure (1 to 4) and each group compared between E12 and E16 NSPCs. N-glycan species containing sialic acid or fucose residues were grouped to compare sialic acid or fucose containing N-glycans between E12 and E16 NSPCs.

Flow cytometry

Live E12, E16, GlcNAc-treated E12 NSPCs, or DEP sorted cells from E12 NSPCs were dissociated using NeuroCult and washed 3 times with 5% BSA in PBS. For labeling with lectins, 300,000 cells were re-suspended in 20 µg/mL FITC-conjugated lectin *Phaseolus vulgaris* leukagglutinin (L-PHA), 20 µg/mL FITC-conjugated lectin *Lens culinaris* agglutinin (LCA), or 40 µg/mL FITC-conjugated *Sambuca nigra* lectin (SNA) (Vector Labs) in 1% BSA and incubated in the dark at 4^{o} C for 1 hour. After washing 3 times with 1x PBS, cells were re-suspended in PBS containing 3 µM propidium iodide, which was used to exclude non-viable cells for analysis. For antibody labeling, cells were re-suspended in 1% BSA with unconjugated-monoclonal antibody against PSA-NCAM (clone 2-2B, Millipore MAB5324) and incubated at 4^{o} C for 30 min. Following washes in 1% BSA, cells were incubated in the dark at 4^{o} C for 30 min with donkey-anti mouse IgM Alexa Fluor 594 (Jackson ImmunoResearch 715-585-140). Cells were additionally stained using the Zombie Green™ Fixable Viability Kit (BioLegend) to exclude non-viable cells in analysis. All cells were analyzed on a BD LSR II flow cytometer, and the data was collected using the BD FACSDIVA software. All data analysis was performed using FlowJo v10.1.

DEP-based sorting of NSPCs

Mouse NSPCs were dissociated prior to sorting by dielectrophoresis (DEP) with non-enzymatic NeuroCult as described above. Dissociated cells were resuspended in DEP buffer, an iso-osmotic solution consisting of 8.5% (w/v) sucrose, 0.3% (w/v) glucose, and adjusted to a final conductivity of 110 µS/cm via addition of RPMI-1640 medium (Flanagan et al., 2008; Lu et al., 2012). DEP buffer conductivity was measured with a conductivity meter (Thermo Orion, Beverly, MA). The final cell concentration was adjusted to $1x10^{6}$ cells/mL for all DEP experiments.

The DEP device used for sorting experiments was fabricated as previously described and appropriate sorting parameters were used so that DEP had no effect on NSPC survival, proliferation or differentiation potential (Lu et al., 2012; Simon et al., 2014). Prior to DEP sorting, the DEP multi-well device was sterilized by UV light for 30-45 minutes, followed by washing with 70% EtOH (v/v), mQ H_2O, 0.05% trypsin-EDTA (v/v), and DEP buffer in sequential order in a sterile biosafety cabinet. Dissociated cells resuspended in DEP buffer were added to each well ($60x10^{5}$ cells per well) followed by a 10 minute incubation to ensure settling of all cells to the bottom of the wells. This was done to make sure the majority of cells were in close proximity to the electrodes. Cells were sorted by applying an AC electric field using a function generator AFG320 (Tektronix, Beaverton, OR) with 3 $V_{peak\text{-}peak}$ at 100 kHz (sorting frequency) for 5 minutes while 3 washes with DEP buffer removed cells not attracted to the electrodes. Control samples include cells exposed to 1 MHz (control frequency) for 5 minutes, since this frequency exposes cells to DEP but does not sort the cells, or cells incubated in DEP buffer without application of the electric field. Cells from these two controls did not differ in any of the analyses. Cells were collected and either processed for RNA analysis or flow cytometry as described above or plated in proliferation medium in 4mm diameter PDMS microwells on glass coverslips coated with pDL/laminin (Nourse et al., 2014). After 24 hours, the medium on the plated cells was switched to differentiation medium and cells were differentiated for 5 days prior to immunocytochemistry with anti-GFAP as described above.

DEP-based capacitance and cell size measurements

NSPCs were dissociated and suspended in DEP buffer as described above. DEP-based membrane capacitance measurements were obtained using the DEP-Well system, as described previously (Hoettges et al., 2008; Labeed et al., 2011). The DEP-Well was observed using a Nikon inverted microscope equipped with a 1.3 Mpixel video camera, and the change in light intensity across the well over time was determined using a MATLAB (The Mathworks Inc, Natick, MA) script. The well was energized with frequencies ranging from 1 kHz–20 MHz at 5 points per decade. Using MATLAB, light intensity measurements were fit to the single shell model (Broche et al., 2005) and the best-fit model (minimum line correlation coefficient 0.98) was used to determine the specific membrane capacitance (Cspec). Cell diameters were measured using ImageJ to analyze phase contrast microscopy images of trypan blue excluding cells in a hemocytometer.

Brain tissue section analysis:

Developing CD-1 mice embryos were collected at embryonic days E10, E12, E16, and E18. The whole embryo was collected for E10 embryos, the head for E12 embryos, and the brain dissected out at E16 and E18. Tissue was placed in 4% paraformaldehyde (PFA) for approximately 18 hours at 4°C then transferred to 30% sucrose in PBS until the tissue was no longer floating. For some antibodies (SOX1, SOX2), tissue was fixed in 4% PFA, 2% saponin for 2 hours at 4°C. Tissue was quickly frozen in Optimal Cutting Temperature (OCT) compound (Tissue-Tek) and stored at -80°C prior to sectioning. Cryosections (20 µm) were taken along the sagittal plane using a Leica research cryostat (Leica CM3050 S) and mounted on SuperFrost glass slides. Sections were washed with PBS and blocked for 20 min at room temperature with 3% BSA in PBS for lectin histochemistry or 5% donkey serum in PBS for antibody staining, with both solutions containing 0.1% Triton-X 100. For lectin staining, sections were incubated with diluted lectin in blocking solution for 1 hour at room temperature in a humidified chamber. For antibody staining, sections were incubated with primary antibody in blocking solution for 18 hours at 4°C in a humidified chamber then with secondary antibody for 1 hour at room temperature. All sections were counterstained with Hoechst 33342 nuclear dye (Thermo Fisher Scientific) and mounted using VectaShield (Vector Labs). Lectins included FITC-conjugated lectin *Phaseolus vulgaris* leukagglutinin (L-PHA) at 20 µg/mL (Vector Labs). Primary antibodies included goat anti-SOX1 IgG (Santa Cruz Biotechnology SC17318) at 1:50, goat anti-SOX2 IgG (Santa Cruz Biotechnology SC17320) at 1:200, goat-anti DCX (C-18) IgG (Santa Cruz Biotechnology SC8066) at 1:200, mouse anti-MAP2 IgG (Sigma M9942) at 1:200. Secondary antibodies included donkey anti-mouse Alexa Fluor 555 and donkey anti-goat Alexa Fluor 555 (Thermo Fisher Scientific A31570 and A21432) at 1:500. Images of the developing dorsal forebrain surrounding the lateral ventricle were taken using a Nikon Eclipse Ti-E fluorescent microscope at 20x magnification and the NIS image capturing software. The cortical plate (CP) and ventricular zone/subventricular zone (VZ/SVZ) were distinguished by MAP2/DCX for neurons in the CP and SOX1/SOX2 staining for NSPCs in the VZ/SVZ. A measuring box generated in ImageJ was used to quantify the average signal intensity in 10 randomly selected areas within each of the given regions and lectin-stained blood vessels were excluded from analysis. Maximum and minimum intensity values were recorded for each analyzed box and the minimum value was subtracted from the maximum to control for variations in staining intensity across different staining batches. One brain from a litter represented one biological repeat and at least 3 brains were analyzed for each embryonic stage.

Supplemental References

GeneCards: The Human Gene Database. In: Weizmann Institute of Science.

Arulmoli J, Wright HJ, Phan DT, Sheth U, Que RA, Botten GA, Keating M, Botvinick EL, Pathak MM, Zarembinski TI, Yanni DS, Razorenova OV, Hughes CC, Flanagan LA (2016) Combination scaffolds of salmon fibrin, hyaluronic acid, and laminin for human neural stem cell and vascular tissue engineering. Acta Biomater *43*,122-138.

Broche L, Labeed F, Hughes M (2005) Extraction of dielectric properties of multiple populations from dielectrophoretic collection spectrum data. Physics in Medicine and Biology *50*,2267-2274.

Cheng X, Hsu CM, Currle DS, Hu JS, Barkovich AJ, Monuki ES (2006) Central roles of the roof plate in telencephalic development and holoprosencephaly. J Neurosci *26*,7640-7649.

Flanagan LA, Lu J, Wang L, Marchenko SA, Jeon NL, Lee AP, Monuki ES (2008) Unique dielectric properties distinguish stem cells and their differentiated progeny. Stem Cells *26*,656-665.

Goecks J, Nekrutenko A, Taylor J, Team G (2010) Galaxy: a comprehensive approach for supporting accessible, reproducible, and transparent computational research in the life sciences. Genome Biol *11*,R86.

Grigorian A, Lee SU, Tian W, Chen IJ, Gao G, Mendelsohn R, Dennis JW, Demetriou M (2007) Control of T Cell-mediated autoimmunity by metabolite flux to N-glycan biosynthesis. J Biol Chem *282*,20027-20035.

Hoettges KF, Hübner Y, Broche LM, Ogin SL, Kass GE, Hughes MP (2008) Dielectrophoresis-activated multiwell plate for label-free high-throughput drug assessment. Anal Chem *80*,2063-2068.

Labeed FH, Lu J, Mulhall HJ, Marchenko SA, Hoettges KF, Estrada LC, Lee AP, Hughes MP, Flanagan LA (2011) Biophysical characteristics reveal neural stem cell differentiation potential. PLoS One *6*,e25458.

Lee SU, Grigorian A, Pawling J, Chen IJ, Gao G, Mozaffar T, McKerlie C, Demetriou M (2007) N-glycan processing deficiency promotes spontaneous inflammatory demyelination and neurodegeneration. J Biol Chem *282*,33725-33734.

Lissner MM, Thomas BJ, Wee K, Tong AJ, Kollmann TR, Smale ST (2015) Age-Related Gene Expression Differences in Monocytes from Human Neonates, Young Adults, and Older Adults. PLoS One *10*,e0132061.

Lu J, Barrios CA, Dickson AR, Nourse JL, Lee AP, Flanagan LA (2012) Advancing practical usage of microtechnology: a study of the functional consequences of dielectrophoresis on neural stem cells. Integr Biol *4*,1223-1236.

Mortazavi A, Williams BA, McCue K, Schaeffer L, Wold B (2008) Mapping and quantifying mammalian transcriptomes by RNA-Seq. Nat Methods *5*,621-628.

Nourse JL, Prieto JL, Dickson AR, Lu J, Pathak MM, Tombola F, Demetriou M, Lee AP, Flanagan LA (2014) Membrane biophysics define neuron and astrocyte progenitors in the neural lineage. Stem Cells *32*,706-716.

Simon MG, Li Y, Arulmoli J, McDonnell LP, Akil A, Nourse JL, Lee AP, Flanagan LA (2014) Increasing label-free stem cell sorting capacity to reach transplantation-scale throughput. Biomicrofluidics *8*,064106.

Trapnell C, Williams BA, Pertea G, Mortazavi A, Kwan G, van Baren MJ, Salzberg SL, Wold BJ, Pachter L (2010) Transcript assembly and quantification by RNA-Seq reveals unannotated transcripts and isoform switching during cell differentiation. Nat Biotechnol *28*,511-515.

Varki A (2009) Essentials of Glycobiology, 2 Edition. Cold Spring Harbor, New York: Cold Spring Harbor Laboratory Press.